

Selected Papers

Trimethylsumanene: Enantioselective Synthesis, Substituent Effect on Bowl Structure, Inversion Energy, and Electron Conductivity

Shuhei Higashibayashi,¹ Ryoji Tsuruoka,¹ Yarasi Soujanya,² Uppula Purushotham,²
G. Narahari Sastry,² Shu Seki,³ Takeharu Ishikawa,⁴ Shinji Toyota,⁴ and Hidehiro Sakurai*¹

¹Research Center for Molecular Scale Nanoscience, Institute for Molecular Science, Myodaiji, Okazaki, Aichi 444-8787

²Molecular Modeling Group, Indian Institute of Chemical Technology, Tarnaka, Hyderabad 500607, India

³Department of Applied Chemistry, Graduate School of Engineering, Osaka University, 2-1 Yamada-oka, Suita, Osaka 565-0871

⁴Department of Chemistry, Faculty of Science, Okayama University of Science, 1-1 Ridaicho, Kita-ku, Okayama 700-0005

Received October 3, 2011; E-mail: hsakurai@ims.ac.jp

C_3 symmetric chiral trimethylsumanene was enantioselectively synthesized through Pd-catalyzed *syn*-selective cyclotrimerization of an enantiomerically pure iodonorbornenone, ring-opening/closing olefin metathesis, and oxidative aromatization where the sp^3 stereogenic center was transmitted to the bowl chirality. Chiral HPLC analysis/resolution of the derivatives were also achieved. Based on theoretical calculations, the columnar crystal packing structure of sumanene and trimethylsumanene was interpreted as due to attractive electrostatic or CH- π interaction. According to the experimental and theoretical studies, the bowl depth and inversion energy were found to increase on methylation for sumanene in contrast to corannulene. Dissimilarities of the effect of methylation on the bowl structure and inversion energy of sumanene and corannulene were ascribed to differences in steric repulsion. A double-well potential model was fitted to the bowl structure–inversion energy correlation of substituted sumanenes, with a small deviation. The effects of various substituents on the sumanene structure and bowl-inversion energy were analyzed by density functional theory calculations, and it was shown that the bowl rigidity is controlled by a combination of electronic and steric effects of the substituents. The electron conductivity of trimethylsumanene was investigated by time-resolved microwave conductivity method, compared with that of sumanene.

In the wake of the discovery of fullerene, the chemical and physical properties of buckybowls have attracted a great deal of interest because of their unique bowl-shaped π -conjugated structure.^{1–3} The science of buckybowls has grown as a result of the development of practical routes for the synthesis of compounds such as sumanene (**1**)⁴ and corannulene (**2**)⁵ (Figure 1). Sumanene (**1**), which is the smallest C_{3v} symmetric buckybowl, was first synthesized by solution-phase method

in 2003. Since then, the chemical and physical properties of sumanenes have been studied, including its bowl structure,^{6a} face selectivity,^{6a} bowl-inversion energy,^{4,6b,6c} crystal packing,^{6a} electron conductivity,^{6d} metal complexes,^{6e–6h} and optical properties.⁶ⁱ Sumanene derivatives, such as heterasumanenes,⁷ have also been studied. With this background knowledge, we studied five aspects of C_3 symmetric trimethylsumanene (**3**), as listed below.

Direct Selective Synthesis of C_3 Symmetric Substituted Sumanenes. One of the major difficulties in studying the properties of sumanene (**1**) is that of selective synthesis of its derivatives. Because sumanene is C_{3v} symmetric, the selective synthesis of C_3 symmetric trisubstituted derivatives through functionalization at either methylene or benzene is difficult to achieve. Functionalization of the parent compound **1** results in mixtures of regioisomers, with the desired C_3 symmetric derivatives as minor products that are difficult to separate.^{6c,6i} Because of the importance of C_3 symmetric trisubstituted derivatives for studies on the physical properties of sumanene (**1**) and its derivatives or for further transformation into π -conjugated derivatives, functionalized sumanenes have to be

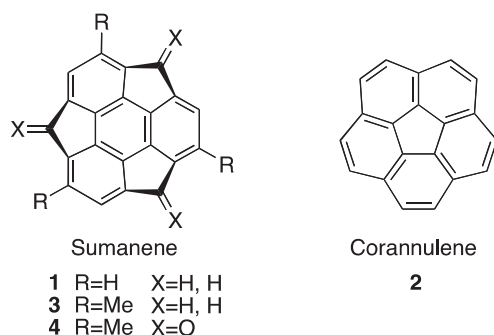


Figure 1. Sumanenes and corannulene.

prepared by a direct route, rather than by derivatization of **1**. Because gas-phase methods (flash vacuum pyrolysis) cannot be used in the case of substituted buckybowls, a solution-phase method is the only available route.¹ We will report full details of a direct selective synthesis of C_3 symmetric trimethylsumanene (**3**) by a solution-phase route.⁸

Chirality Control of Chiral Buckybowls. Because of their three-dimensional bowl structure, buckybowls can possess chirality, *bowl chirality*, in a similar manner to chiral fullerenes or carbon nanotubes. Bowl chirality can be induced by the π -conjugated skeleton itself (as, for example, in hemifullerene), by the introduction of substituents, or by the replacement of skeletal carbons by heteroatoms (as in heterabuckybowls). Although many buckybowls possess this bowl chirality, no enantioselective synthesis or even a resolution of a racemate has been reported to date.^{9,10} Needless to say, the primary problem of enantioselective synthesis of buckybowls is that of introducing homochirality; a secondary problem that occurs with buckybowls with relatively low bowl-inversion energies is that of racemization through bowl inversion. These problems must be overcome if we are to achieve an enantioselective synthesis of a trisubstituted sumanene. In addition to the direct selective synthesis of trimethylsumanene (**3**), we have succeeded in controlling the bowl chirality of **3** by means of a chiral transmission method. Racemization was inhibited by performing operations and derivatizations at low temperatures.^{8a} We also succeeded in resolving racemic trimethylsumanenetrione (**4**) by means of chiral HPLC.^{8b} With the enantiomerically pure or enantiomerically enriched chiral buckybowl in hand, the bowl-inversion energy could be easily determined by measuring the racemization kinetics by means of circular dichroism spectroscopy, rather than by NMR methods, which can only be used to determine the bowl-inversion energy of buckybowls with diastereotopic protons.

Substituent Effects on the Bowl Structure and the Bowl-Inversion Energy. Bowl inversion is one of the unique properties of buckybowls, and it has been extensively studied since the determination of the bowl-inversion energy of a corannulene derivative by Scott and co-workers.^{5b} The effects of substituents on the bowl structure and the correlation between the bowl structure and the inversion energy of corannulene (**2**) with that of many substituted corannulenes have been studied by Siegel and co-workers.¹¹ However, the corresponding properties of substituted sumanenes have not been studied, mainly because of limitations on the derivatization of these compounds. On the basis of the experimental bowl structures of sumanene (**1**) and trimethylsumanene (**3**) and studies on the bowl-inversion energies of **1**, **3**, and **4**, we studied substituent effects on the sumanene skeleton as well as the structure–inversion energy correlation by means of combinations of calculated data for these compounds. We also discuss the differences between sumanene and corannulene.

Theoretical Calculations to Corroborate the Experimental Observations. We describe a systematic computational approach involving density functional theory (DFT)-based calculations to corroborate our experimental results and to delineate the various factors responsible for controlling the structure and rigidity of the compounds in question. The stacking interactions of molecules in columnar crystal structure

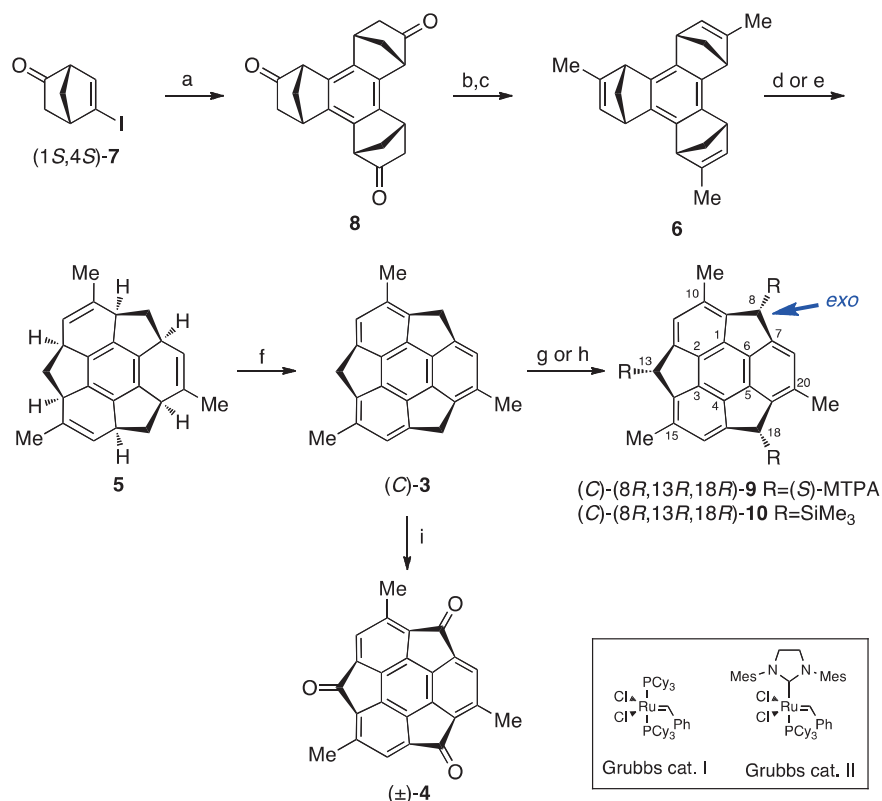
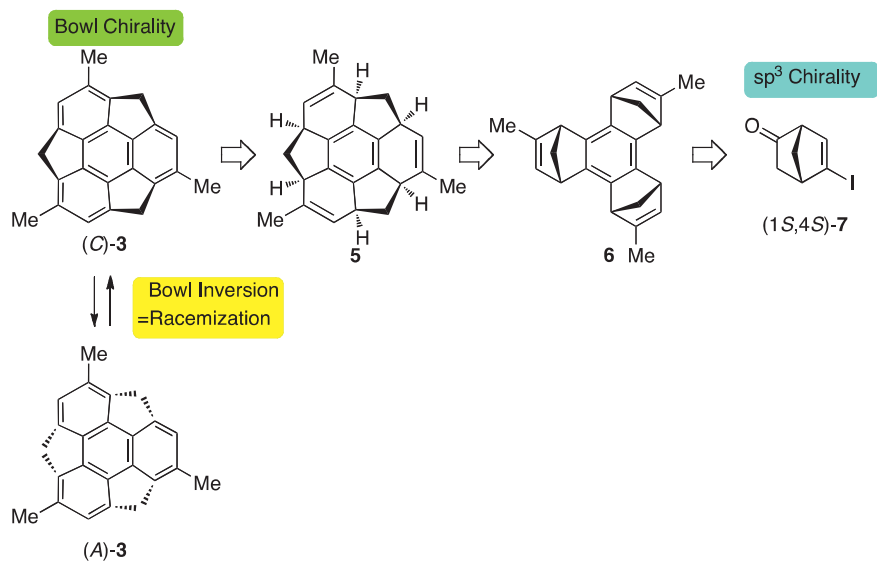
of **1** and **3** are analyzed by theoretical calculations. Substituent effects on the sumanene skeleton are studied with experimental data, and the effects of various substituents are predicted by means of calculations from first principles.

Electron Conductivity. Sumanene (**1**) has a columnar crystal packing structure in which the molecules are stacked in a convex-to-concave fashion with all the columns oriented in the same direction. Because of its stacking structure, sumanene has a high electron mobility ($0.75 \text{ cm}^2 \text{ V}^{-1} \text{ s}^{-1}$) with a large anisotropy (9.2 times) along the column axis, as measured by time-resolved microwave conductivity (TRMC).^{6d} Although the columnar crystal packing structures of buckybowls must be correlated with their electronic properties,^{1d} these correlations have not been studied until now. Transfer integrals of LUMO orbitals in the contacting buckybowls are predicted to play a crucial role in the effective transport of electrons along the columnar stacking axes, and unidirectional stacking may provide a ratchet-type potential for electrons because of the asymmetric lobes of the LUMO orbitals in the convex-to-concave sides of the buckybowls. Because trimethylsumanene (**3**) was found to possess a columnar crystal structure with neighboring columns aligned in opposite directions, in contrast to **1**, the effect of column alignment on the electron transport properties of **3** was studied by the TRMC method.

Results and Discussion

Enantioselective Synthesis of Trimethylsumanene (3**) and Determination of Its Bowl-Inversion Energy.** Our strategy for the enantioselective synthesis of C_3 symmetric trimethylsumanene (**3**) is based on a conversion involving a *syn*-selective cyclotrimerization of an enantiomerically pure norbornene derivative to give a C_3 symmetric *syn*-tris(norbornadieno)benzene derivative, ring-opening/closing metathesis reactions to form the nonconjugated bowl structure, and aromatization to the conjugated bowl structure in which the chirality of the sp^3 stereogenic center is transformed into bowl chirality (Scheme 1).^{8a} In the final chirality-transmission process, the bowl-inversion energy of (*C*)-**3** must be taken into account, because inversion from (*C*)-**3** to (*A*)-**3** corresponds to a racemization process for the chiral buckybowl.¹² The bowl-inversion energy of **3** was estimated to be ca. 21 kcal mol^{-1} by comparison between the experimental value ($\Delta G^\ddagger = 20.3 \text{ kcal mol}^{-1}$ (303 K)^{6b}) of **1** and the calculated values (B3LYP/6-311+G(d,p): 18.3 and $19.2 \text{ kcal mol}^{-1}$) of **1** and **3**, respectively. Because this energy corresponds to a half-lifetime for racemization of about 2 h at 0°C , the aromatization step must be carried out at a low temperature. We surmised that the bowl-shaped structure of **5** might be constructed from the *syn*-tris(norbornadieno)benzene derivative **6** by a ring-opening/closing olefin metathesis approach and that the *syn*-tris(norbornadieno)benzene derivative **6** might be obtained by *syn*-selective cyclotrimerization of the chiral halonorbornene derivative (1*S*,4*S*)-**7**. By adopting this approach, the bowl chirality of **3** is controlled by the sp^3 stereogenic center of the starting norbornene derivative **7**.

The C_3 symmetric *syn*-tris(oxonorborneno)benzene **8** was prepared by Pd-catalyzed *syn*-selective cyclotrimerization of enantiomerically pure iodonorbornenone (1*S*,4*S*)-**7** (Scheme 2), as developed by our group.^{8a,13} Methyl groups were introduced



Scheme 2. Synthesis of trimethylsumanene (**3**) and trimethylsumanenetrione (**4**). Reagents and conditions: (a) Pd(OAc)₂ 5 mol %, PPh₃ 10 mol %, Bu₄NOAc 1000 mol %, Na₂CO₃, 4 Å MS, 1,4-dioxane, 100 °C, 2 h, 49% (*syn/anti* = 95:5); (b) NaN(SiMe₃)₂ 350 mol %, (2,6-Me₂C₆H₃O)₂P(O)Cl 350 mol %, P(O)(NMe₂)₃ 350 mol %, THF, -80 °C, 75%; (c) Pd(OAc)₂ 5 mol %, PCy₃·HBF₄ 10 mol %, MeMgI 400 mol %, THF, 40 °C, 2 h, 72%; (d) Grubbs catalyst I 50 mol %, CH₂Cl₂ (0.011 M), under ethylene, 40 °C, 6 h, then Grubbs catalyst II 50 mol %, CH₂Cl₂ (0.034 M), 40 °C, 12 h, 24%; (e) Grubbs catalyst II 50 mol %, toluene (0.1 M), (*Z*)-oct-4-ene 1000 mol %, sealed tube, 90 °C, 12 h, 26%; (f) DDQ 600 mol %, CH₂Cl₂, 0 °C, 1 min, 68%; (g) LDA 600 mol %, THF, -40 °C, then (*R*)-PhC(CF₃)(OMe)COCl ((*R*)-MTPACl) 1000 mol %, (*C*)-(8*R*,13*R*,18*R*)-**9**, 17%; (h) LDA 600 mol %, THF, -40 °C, then Me₃SiCl 1000 mol %, (*C*)-(8*R*,13*R*,18*R*)-**10**, 34%; (i) (±)-**3**, NaN(SiMe₃)₂ 450 mol %, DMF, O₂ atmosphere, -40 °C, 5 min, (±)-**4**, 26%.

by Pd-catalyzed cross-coupling of MeMgI with an alkenyl phosphate prepared from **8** to give the trimethylated *syn*-tris(norbornadieno)benzene **6**. In the case of the synthesis of sumanene (**1**), Grubbs catalyst I worked for both the ring-opening and ring-closing metathesis reactions of the unsubstituted *syn*-tris(norbornadieno)benzene under an ethylene atmosphere, giving hexahydrosumanene. In contrast, treatment of **6** with Grubbs catalyst I under an ethylene atmosphere resulted in a mixture of ring-opened reaction products exclusively. Grubbs catalyst II was therefore adopted for the ring-closing reaction of the mixture, giving the desired hexahydrotrimethylsumanene **5** in 24% yield. Furthermore, Grubbs catalyst II was effective in the ring-opening metathesis reaction as well as the ring-closing reaction, which allowed us to use a single catalyst for the tandem ring-opening/closing metathesis reaction. When ethylene gas was used as the alkene source for the ring-opening reaction, operations had to be performed under dilute conditions to dissolve ethylene gas into solution in order to prevent polymerization of the substrate. After screening the reaction conditions, we selected liquid (*Z*)-oct-4-ene (bp 122 °C) as the alkene source to improve solubility and to prolong the lifetime of the catalyst. Because a higher temperature was necessary for the olefin metathesis reaction to proceed with (*Z*)-oct-4-ene, toluene was used as solvent instead of dichloromethane. By adopting this combination of conditions, we obtained **5** in 26% yield from **6** in one-pot operation using Grubbs catalyst II and (*Z*)-oct-4-ene in toluene in a sealed tube. The final aromatization of **5** was carried out with an excess of 2,3-dichloro-5,6-dicyano-1,4-benzoquinone (DDQ) at 0 °C for a short time (1 min) to prevent racemization of **3**. The resulting reaction mixture was quickly purified by silica gel chromatography at a low temperature (below –20 °C) to afford the desired chiral bucky bowl **3**.^{8a}

The chirality of thus-obtained **3** was confirmed by circular dichroism (CD) spectroscopy. Because the bowl inversion causes rapid racemization at room temperature, the CD spectrum of **3** was recorded at –40 °C. As expected, the CD spectrum was observed at –40 °C as shown in Figure 2A and the intensity of the CD spectrum scarcely changed at –40 °C. The absolute configuration of thus-prepared **3** from (1*S*,4*S*)-**7** is assigned to be (*C*)-**3** because the bowl structure of **5** is thought to be maintained during the oxidation step to **3**. The absolute

configuration was supported by the comparison between the observed CD spectrum and the calculated one of (*C*)-**3** by TD-DFT calculation (Supporting Information). In contrast to the CD spectrum observed at –40 °C, a gradual decrease in the intensity of the CD spectrum was observed at 10 °C (Figure 2B). By following the decay of the CD spectra at 247 and 282 nm at 10 °C, we determined the rate constant of the racemization/bowl inversion and the bowl-inversion energy of **3** in MeCN to be $\Delta G^\ddagger = 21.6 \text{ kcal mol}^{-1}$ (283 K) by Eyring equation,^{8a} which is 1.3 kcal mol^{–1} higher than that of sumanene (**1**) ($\Delta G^\ddagger = 20.3 \text{ kcal mol}^{-1}$ (303 K)).^{6b}

Since it is difficult to determine the enantiomeric excess (ee) of (*C*)-**3** directly due to the racemization derived from the relatively low bowl-inversion energy, we estimated the ee of (*C*)-**3** by two methods involving derivatization. Through the generation of trianion at the three benzylic positions of sumanene (**1**) followed by the addition of electrophiles, substituents can be selectively introduced at the benzylic positions with *exo*-orientation¹⁴ to the bowl structure of sumanene as previously reported.^{6a,6b} By adopting the derivatization method, the sample of (*C*)-**3**, which was kept at low temperature as mentioned above to avoid racemization, was subjected to the conditions introducing (*S*)-MTPA (PhC(CF₃)(OMe)CO) groups or SiMe₃ groups at the benzylic positions at low temperature (–40 °C) (Scheme 2). (*S*)-MTPA groups or SiMe₃ groups are selectively introduced with *exo*-orientation¹⁴ without the bowl inversion of (*C*)-**3**. Thus, this derivatization affords the corresponding derivatives (*S*)-MTPA-(*C*)-(8*R*,13*R*,18*R*)-**9** and (*C*)-(8*R*,13*R*,18*R*)-**10** bearing *exo*-oriented substituents, respectively (Scheme 2). The absolute configuration was further supported by the comparison between the observed CD spectrum and the calculated one of (*C*)-(8*R*,13*R*,18*R*)-**10** by TD-DFT calculation (Supporting Information). The introduction of the substituents induces new stereogenic centers at the benzylic positions. As a result, the bowl inversion cannot cause the racemization but result instead in the diastereomerization between the *exo*-orientation and the *endo*-orientation of substituents (Scheme 3). The diastereomerization through the bowl inversion, however, is negligible because the bulky substituents significantly favor the *exo*-orientation over the *endo*-orientation.^{6a,14} DFT calculation (B3LYP/6-31G(d)) of **10** shows that the *exo*-orientation of substituents is 20.2 kcal mol^{–1} more stable than the *endo*-orientation. The ¹H NMR spectra of **9** and **10** do not show the existence of diastereomers with *endo*-substituents formed through bowl inversion, either. Thus, the ratio of (*C*)-(8*R*,13*R*,18*R*)-**9** or **10** from (*C*)-**3** and (*A*)-(8*S*,13*S*,18*S*)-**9** or **10** from (*A*)-**3** bearing *exo*-substituents can be analyzed without racemization or diastereomerization through the bowl inversion. In the case of **9**, the formation of (*S*)-MTPA-(*C*)-(8*R*,13*R*,18*R*)-**9** from (*C*)-**3** and (*S*)-MTPA-(*A*)-(8*S*,13*S*,18*S*)-**9** from the contaminant (*A*)-**3**, which correspond to the relevant diastereomers, permits the determination of the diastereomeric excess (de) of **9** to be 90% by means of ¹H NMR analysis.^{8a} In contrast, (*C*)-(8*R*,13*R*,18*R*)-**10** and (*A*)-(8*S*,13*S*,18*S*)-**10** are enantiomers that can be discriminated by means of chiral HPLC analysis. Indeed, they were resolved by using Daicel Chiralpak IA with 2-propanol as the eluent (Figure 3A). The ee of **10** was determined to be 89%, which agrees with the value for **9**. Racemic **10** was also resolved to

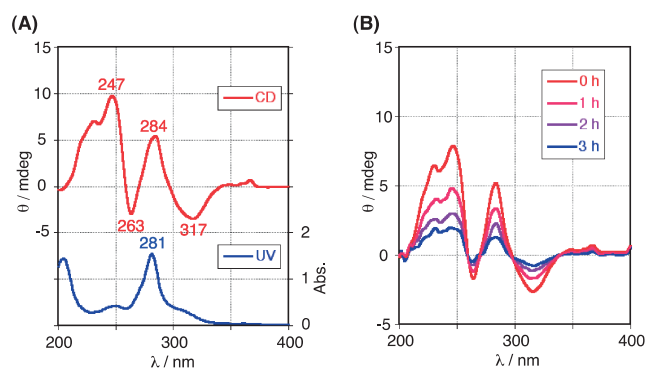
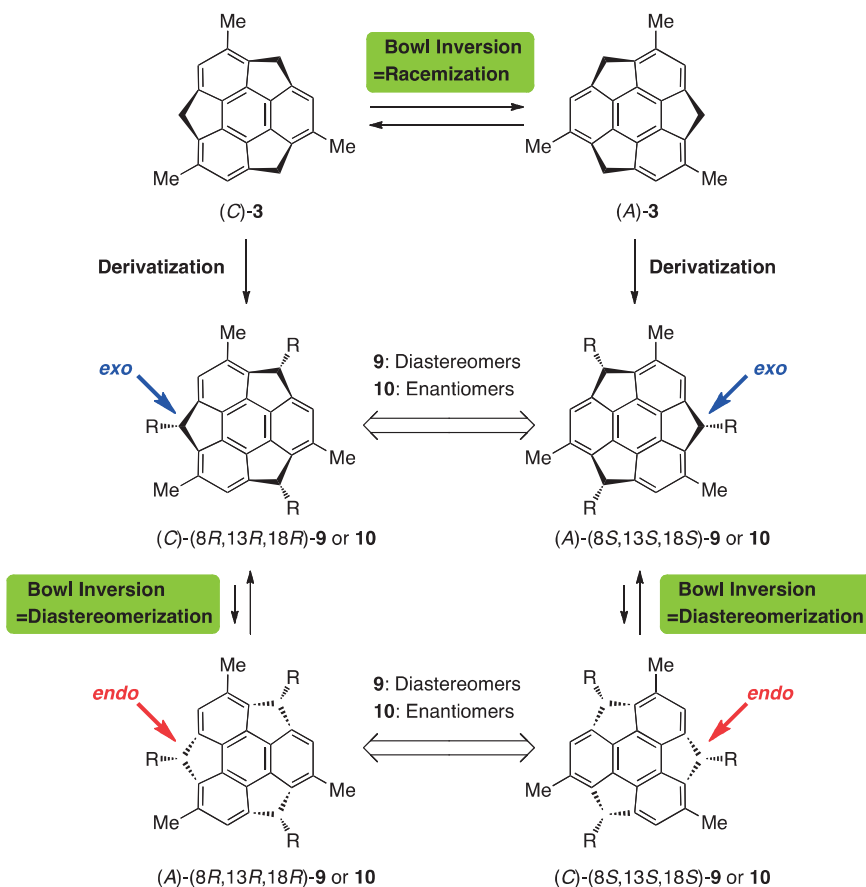


Figure 2. (A) CD spectrum of (*C*)-**3** in MeCN at –40 °C (red line) and UV spectrum of (\pm)-**3** in MeCN at rt (blue line); (B) decay of CD spectra of (*C*)-**3** in MeCN at 10 °C during 3 h.



Scheme 3. Relationship of stereoisomers of trimethylsumanene derivatives through bowl inversion.

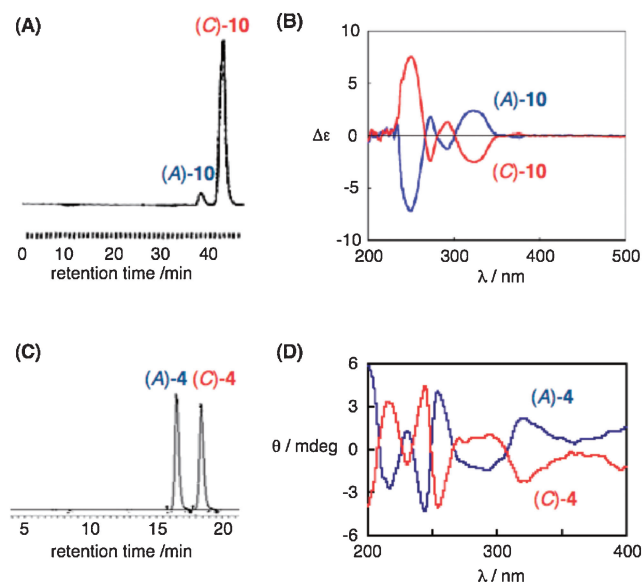


Figure 3. (A) Chiral HPLC (Daicel Chiralpak IA, 2-propanol, rt) analysis of (C)-10. (B) CD spectra of (C)-10 and (A)-10 in CHCl₃ at rt. (C) Chiral HPLC (Daicel Chiralpak IA, 2-propanol/hexane = 5/95, 9 °C) analysis of (±)-4. (D) CD spectra of (C)-4 and (A)-4 in MeCN at rt.

give the corresponding enantiomers, and their CD spectra were recorded (Figure 3B).^{8b} From the results for **9** and **10**, the ee of (C)-**3** was estimated to be >89%. Because the ee of the starting

material was >99%, it was apparent that only a relatively small amount of racemization had occurred during the aromatization from **5** to **3** and subsequent purification step of **3**.

Synthesis and Chiral HPLC Resolution of Trimethylsumanenetrione (4). Chiral HPLC resolution of **10** is possible because the presence of the sp³ stereogenic centers in addition to the bowl chirality prevents racemization of the compound by bowl inversion. In contrast, the resolution of a buckybowl with exclusive bowl chirality, such as trimethylsumanene (**3**), is difficult to achieve because of the rapid racemization of the compound. However, if a buckybowl has a high bowl-inversion energy, the slow rate of racemization on the HPLC time-scale might permit the resolution of the racemic buckybowl by means of chiral HPLC. Separation of racemic chiral buckybawls might therefore be another effective strategy for obtaining an enantiomerically pure or an enantiomerically enriched sample for the determination of the bowl-inversion energy by CD spectral measurements. (±)-Trimethylsumanenetrione (**4**), prepared by oxidation of (±)-**3** (Scheme 2), was a candidate for this process because its bowl-inversion energy was estimated to be ca. 23.5 kcal mol⁻¹ by comparison between the experimental value ($\Delta G^\ddagger = 20.3$ kcal mol⁻¹ (303 K))^{6b} of **1** and the calculated values (B3LYP/6-311+G(d,p): 18.3 and 21.5 kcal mol⁻¹) of **1** and **4**, which corresponds to a half-life of about 44 h, even at 10 °C.^{8b} This value could be high enough to permit the isolation of enantiomerically enriched **4** by means of chiral HPLC. Furthermore, the bowl-inversion energy of **4** cannot be determined by an NMR technique, because **4** does not contain

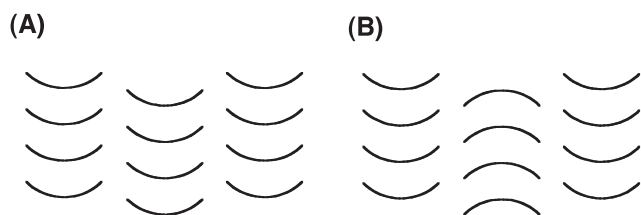


Figure 4. Molecular packing of buckybowls in crystals.

the diastereotopic protons at the benzylic positions that are required to examine the bowl-inversion rate by NMR. As we expected, resolution of **4** was achieved by using Daicel Chiralpak IA at 9 °C with hexane/2-propanol = 95/5 as the eluent, giving samples of each of the enantiomerically enriched forms of **4** (Figures 3C and 3D). By using the resulting enantiomerically enriched samples of **4**, we determined the rate constant of the racemization/bowl inversion and the bowl-inversion energy to be $\Delta G^\ddagger = 23.4 \text{ kcal mol}^{-1}$ (303 K) in MeCN and $23.3 \text{ kcal mol}^{-1}$ (303 K) in CH_2Cl_2 by Eyring equation^{8b} from the time-dependent decay of the intensity of the CD spectra at 255 nm at 30 °C; these values are higher than the corresponding value for **3** ($\Delta G^\ddagger = 21.6 \text{ kcal mol}^{-1}$ (283 K)).^{8a}

Crystal Packing Structure of Trimethylsumanene.

Siegel and Wu classified the molecular-packing structures of nine different crystalline buckybowls into three types; (A) columnar convex-to-concave stacks with all columns in a constant direction, (B) columnar convex-to-concave stacks with neighboring columns in opposite directions, and (C) noncolumnar structures (Figure 4; type C is omitted) in their review.^{1e} Sumanene (**1**) possesses a columnar packing structure with unidirectional columns of type A,^{6a} where the bowls are stacked without slipping from side to side. The origin of the columnar packing structure of sumanene is one of our interests as well as the substituent effect on the packing. The difference of packing structure also must be correlated to the properties in the solid state such as the electronic properties. A single crystal of (\pm)-trimethylsumanene (**3**) for X-ray crystallographic analysis was obtained by crystallization from tetrahydrofuran. ORTEP drawings of (\pm)-**3** are shown in Figure 5. These show a columnar packing structure in which the molecules are stacked in a convex-to-concave fashion without slipping from side to side. In contrast to the columnar crystal packing of **1**, neighboring columns of (\pm)-**3** are oriented in opposite directions, which belongs to type B (Figure 4). (*A*)-**3** and (*C*)-**3** are stacked alternatively at a distance of 3.96 Å with a 46.8° twist angle in the column; the corresponding values for sumanene (**1**) are 3.86 Å and 55.5°, respectively.^{6a} The twist angles of **1** and **3** result in the stacking of the benzene rings and the cyclopentadiene rings. The twist angles of **1** and **3** can be explained in terms of a combination of an intermolecular repulsive interaction and an attractive interaction. The repulsive interaction corresponds to the intermolecular steric repulsion between the *endo*-H and *exo*-H atoms of the cyclopentadiene rings. Stacking with a 0° twist angle would lead to a significant intermolecular repulsion between these hydrogen atoms. The observed twist angles of **1** and **3** prevent this steric repulsion. The attractive interaction can be interpreted to be the intermolecular electrostatic interactions between benzene rings and cyclopentadiene rings or the intermolecular CH- π interactions

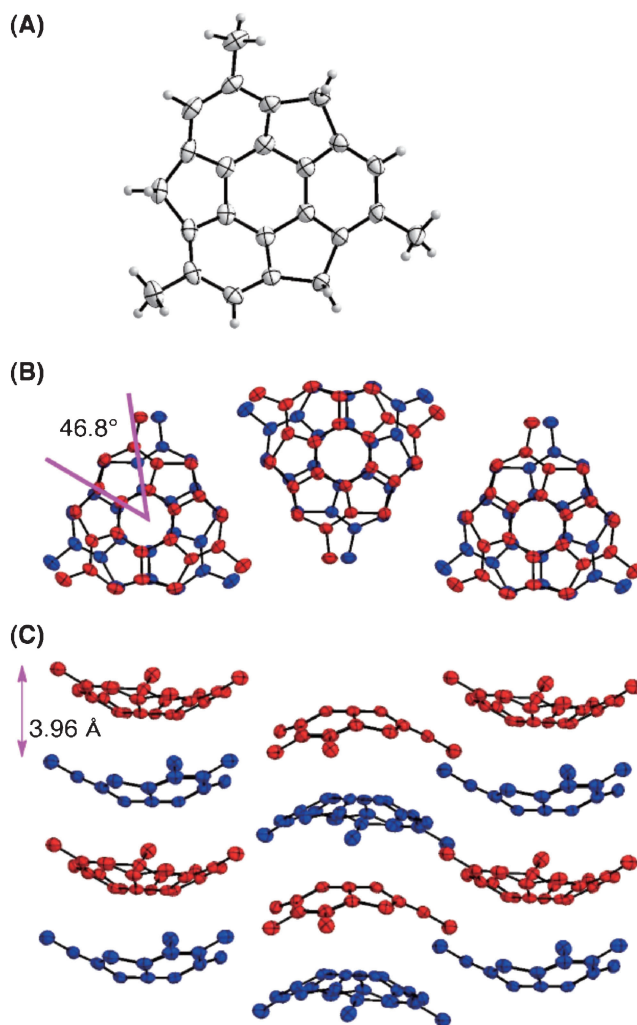


Figure 5. (A) ORTEP drawings of X-ray crystallographic analysis of (\pm)-**3**, (B) top view, (C) side view, shown at the 50% probability level.

between *endo*-H atoms of the cyclopentadiene rings and the benzene rings. Analysis of the electrostatic potentials (ESP) generated for the sumanene monomer indicates that the benzene rings are electron rich and that the cyclopentadiene rings are electron deficient (Figure 6). The observed twist angles of **1** and **3** can induce favorable electrostatic interactions between the electron-rich benzene ring and the electron-deficient cyclopentadiene ring, although the ESP-based explanation for the intermolecular interaction in crystal is not conclusive in all cases.¹⁵ Another explanation for twisted stacking involves a possible CH- π interaction,¹⁶ where the *endo*-H atom of the cyclopentadiene ring of the lower bowl points toward the benzene ring of the upper bowl (Figures 7A and 7B). Since the CH- π interaction between cyclopentadiene and benzene has not been reported, the evidence for this kind of CH- π interaction is obtained from a model complex of benzene interacting with cyclopentadiene (Figure 7C). The interaction energy with counterpoise correction for the benzene-cyclopentadiene complex with interacting distance of 3.1 Å is found to be $-4.34 \text{ kcal mol}^{-1}$ at the MP2/cc-pVDZ level. The observed twist angles of **1** and **3** can be correlated to

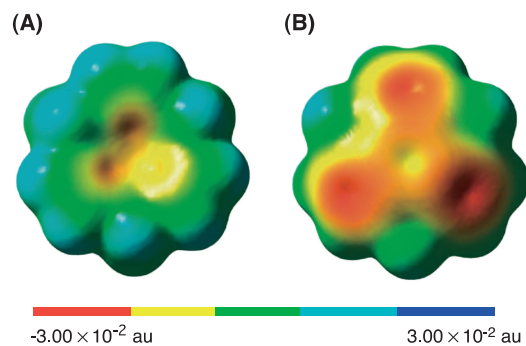


Figure 6. Electrostatic potential (ESP) map plotted onto (A) concave and (B) convex surfaces of sumanene (**1**) (the isosurface at 0.002 au) calculated by using the MP2 density (MP2/cc-pVDZ). Mapping colors from red (-3.00×10^{-2} au) to blue (3.00×10^{-2} au).

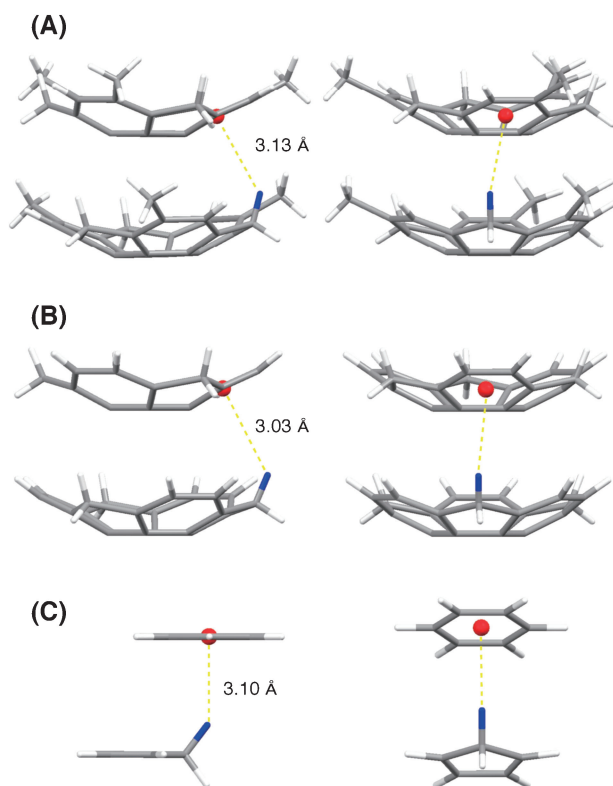


Figure 7. CH- π interactions in (A) crystalline trimethylsumanene (**3**), (B) crystalline sumanene (**1**), and (C) a model complex of benzene interacting with cyclopentadiene, obtained by MP2/cc-pVDZ calculation.

the presence of a CH- π interaction involving the *endo*-H atom of the cyclopentadiene ring and the benzene ring. The repulsive and attractive interactions also cause structural changes of **1** and **3** in the crystal state. The structural changes are discussed in the next section together with differences in the crystal structures of **1** and **3** arising from methylation.

Structural Analysis of Sumanene (1), Trimethylsumanene (3), and Trimethylsumanenetrione (4). To account for the structural differences observed in the crystals of **1** and **3**, and to understand the effects of methylation on the bowl structure and bowl-inversion energy for **3** in comparison

Table 1. Experimental and Calculated (B3LYP/6-311+G(d,p)) Bowl-Inversion Energy (ΔE) and the Differences ($\Delta\Delta E$) of ΔE of **3** or **4** from ΔE of **1**

	Experimental		Calculated	
	ΔE /kcal mol ⁻¹	$\Delta\Delta E$ /kcal mol ⁻¹	ΔE /kcal mol ⁻¹	$\Delta\Delta E$ /kcal mol ⁻¹
1	20.3	0	18.3	0
3	21.6	+1.3	19.2	+0.9
4	23.4	+3.1	21.5	+3.2

with **1** and **4**, we undertook a theoretical study based on DFT. It is important to note that the theoretical calculations are pertinent to properties of a single molecule in the gas phase. Therefore, discrepancies observed between the theory and the crystal structure can be attributed, albeit with careful analysis, to intermolecular interactions resulting from crystal packing.¹⁷ To evaluate the reliability of the calculation method, we calculated the bowl-inversion energies of **1**, **3**, and **4** by optimizing the bowl structure and the flat structure corresponding to the transition state for the bowl inversion at the B3LYP or M05-2X level of theory with a range of basis sets (6-31G(d), 6-311G(d,p), 6-31++G(d,p), 6-311+G(d), 6-311+G(d,p), and cc-pVDZ). Among them, the B3LYP/6-311+G(d,p) method was found to be reliable for the differences of bowl-inversion energies of **3** or **4** from that of **1** (**3**: +0.9, **4**: +3.2 kcal mol⁻¹) to those of experimental values (**3**: +1.3, **4**: +3.1 kcal mol⁻¹) (Table 1). Taking the values of the bowl-inversion energies and the calculation cost into account, we suggest that B3LYP calculations with the 6-311+G(d,p) basis set are suitable for modeling of this class of compounds.

To examine the effects of the methyl groups, carbonyl groups, and intermolecular interactions on the crystal structure in detail, we analyzed the bond length (r), π -orbital axis vector (POAV) pyramidalization angle (ϕ),¹⁸ bowl depth (d), and cone angle (θ) in the calculated and experimental structures of **1**, **3**, and **4** (Figure 8).

The calculated and experimental bond lengths (r_{cal} and r_{exp}) for **1**, **3**, and **4** are shown in Table 2. Instances of differences (>0.003 Å) between the calculated values r_{cal} and experimental values r_{exp} for **1**, **3**, and **4** are presented in Figure 9; with longer and shorter distances highlighted in blue and red, respectively. In the calculations, the flank bond (C7–C8) and the rim bond (C8–C9) of **3** are longer than those of **1** because of the introduction of the methyl groups (Figure 9A). In contrast, the difference (Δr_{exp}) between the experimental bond lengths r_{exp} (**3**) and r_{exp} (**1**) show more complex changes owing to the additional effects of intermolecular interactions in the crystal, although the flank bond (C7–C8) remains longer in all cases (Figure 9C). The difference Δr between r_{exp} and r_{cal} for **1** (Figure 9D) and for **3** (Figure 9E) shows shortening of some bonds, probably as a result of intermolecular interactions in the crystal. It is evident from Figures 9D and 9E that the effects of intermolecular interactions on the bond length of **3** are not identical to those in **1**. Owing to the complex nature of the changes that emerge from a comparison of the experimental and the calculated bond lengths for **1** and **3**, we will restrict our discussion to a comparison of the geometries of Figures 9A

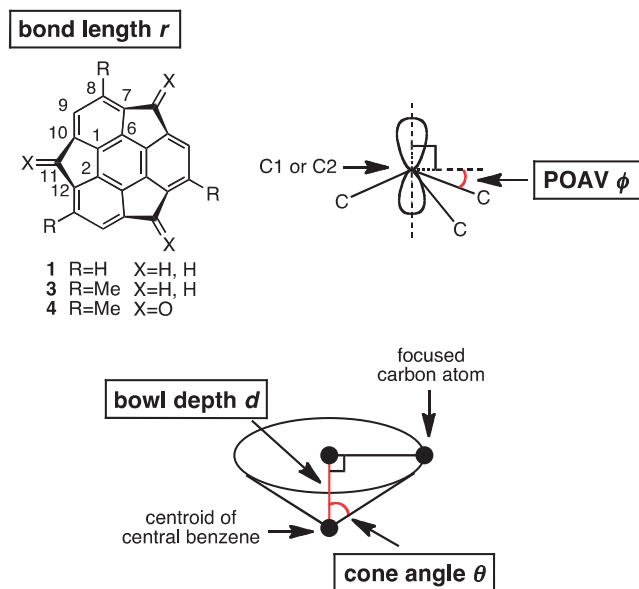


Figure 8. Analyzed parameters: bond length (r), POAV (ϕ), bowl depth (d), and cone angle (θ).

Table 2. Calculated^{a)} and Experimental Bond Lengths (r_{cal} and r_{exp} , respectively) of **1**, **3**, and **4**

Bond	Bond length $r_{\text{cal}}/\text{\AA}$			Bond length $r_{\text{exp}}/\text{\AA}$	
	1	3	4	1	3
C1–C2	1.433	1.433	1.439	1.430	1.433
C1–C6	1.385	1.384	1.376	1.381	1.382
C6–C7	1.397	1.396	1.398	1.395 ^{b)}	1.390
C1–C10	1.397	1.395	1.401	1.395 ^{b)}	1.390
C7–C8	1.397	1.404	1.391	1.398 ^{b)}	1.402
C9–C10	1.397	1.397	1.404	1.398 ^{b)}	1.396
C8–C9	1.430	1.435	1.438	1.430	1.428
C10–C11	1.552	1.552	1.542	1.547	1.551
C11–C12	1.552	1.554	1.544	1.547	1.549

a) B3LYP/6-311+G(d,p). b) Average values between $r(\text{C6–C7})$ and $r(\text{C1–C10})$ and between $r(\text{C7–C8})$ and $r(\text{C9–C10})$, respectively.

and 9C. It is apparent from Figure 9 that, whereas the theoretical calculations predict an elongation of the rim and flank bonds on substitution, crystal packing results in a shortening or shrinking of the spoke bonds as well as an elongation of the rim and flank bonds in **1** and **3**. A comparison of r_{cal} for compounds **4** and **3** shows that the flank bond lengths (C10–C11 and C11–C12) of **4** are shorter than those of **3**, owing to the change from sp^3 to sp^2 hybridization at C11 (Figure 9B).

The POAV angles (ϕ) of **1**, **3**, and **4** are shown in Table 3. The experimental values ϕ_{exp} for **1** and **3** are in close agreement with the calculated values ϕ_{cal} . However, this consistency arises from the nature of this parameter, which does not reflect subtle structural changes. Judging from these values, the methyl group induces a disproportionation only at C1 and C2. In contrast, the structural changes in **4** are sufficiently large to affect the value of ϕ . The introduction of a carbonyl group increases the POAV angle as well as causing a disproportionation at C1 and C2.

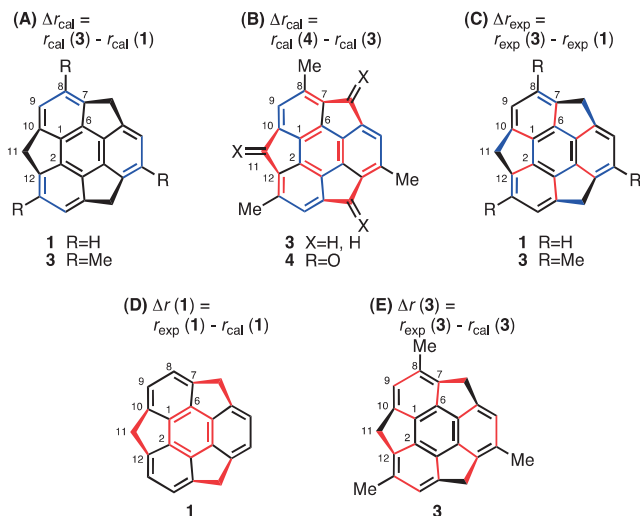


Figure 9. Bond length differences between r_{cal} (B3LYP/6-311+G(d,p)) and r_{exp} for **1**, **3**, and **4**. Lengthening and shortening of bonds ($>0.003 \text{\AA}$) are highlighted by blue and red colors, respectively. (A) Δr between r_{cal} for **3** and r_{cal} for **1**, (B) Δr between r_{cal} for **4** and r_{cal} for **3**, (C) Δr between r_{exp} for **3** and r_{exp} for **1**, (D) Δr between r_{exp} for **1** and r_{cal} for **1**, (E) Δr between r_{exp} for **3** and r_{cal} for **3**.

Table 3. Calculated^{a)} and Experimental π -Orbital Axis Vector (POAV) Pyramidalization Angles of **1**, **3**, and **4**

Position	POAV $\phi_{\text{cal}}/^\circ$			POAV $\phi_{\text{exp}}/^\circ$	
	1	3	4	1	3
C1	8.8	9.1	9.4	8.7 ^{b)}	9.1
C2	8.8	8.6	8.8	8.7 ^{b)}	8.6

a) B3LYP/6-311+G(d,p). b) Average value between C1 and C2.

Table 4. Calculated^{a)} and Experimental Bowl Depths (d_{cal} and d_{exp}) for **1**, **3**, and **4**

Position	Bowl depth $d_{\text{cal}}/\text{\AA}$			Bowl depth $d_{\text{exp}}/\text{\AA}$	
	1	3	4	1	3
C7	0.626	0.630	0.645	0.620 ^{b)}	0.622
C10	0.626	0.628	0.648	0.620 ^{b)}	0.620
C8	1.143	1.154	1.195	1.115 ^{b)}	1.112
C9	1.143	1.146	1.191	1.115 ^{b)}	1.102
C11	0.880	0.891	0.978	0.899	0.913

a) B3LYP/6-311+G(d,p). b) Average value between d (C7) and d (C10) and between d (C8) and d (C9), respectively.

The bowl depths (d) of **1**, **3**, and **4** and the differences in these values Δd are shown in Tables 4 and 5. The difference Δd_{cal} between d_{cal} of **3** and that of **1** suggests that the introduction of methyl groups increases the bowl depth at all positions. On the other hand, the experimental values d_{exp} at C8 and C9 in the crystal of **3** are shallower than those of **1**, whereas d_{exp} at C11 of **3** is deeper than that of **1**. The difference Δd between the experimental d_{exp} and the calculated d_{cal} suggests that the effect of intermolecular interactions on the bowl depths d_{exp} of **3** is similar to that of **1**, which is deeper at C11 and shallower at other positions in the crystal. The

Table 5. Differences^{a)} Δd among Bowl Depths d_{cal} (B3LYP/6-311+G(d,p)) and d_{exp} of **1**, **3**, and **4**

Position	$\Delta d_{\text{cal}}/\text{\AA}$		$\Delta d_{\text{exp}}/\text{\AA}$	$\Delta d = d_{\text{exp}} - d_{\text{cal}}/\text{\AA}$	
	$d(\mathbf{3}) - d(\mathbf{1})$	$d(\mathbf{4}) - d(\mathbf{3})$	$d(\mathbf{3}) - d(\mathbf{1})$	1	3
C7	0.004	0.015	0.002	-0.006	-0.008
C10	0.002	0.020	0.000	-0.006	-0.008
C8	0.011	0.041	-0.003	-0.028	-0.042
C9	0.002	0.045	-0.013	-0.028	-0.044
C11	0.011	0.087	0.014	0.019	0.022

a) Longer and shorter changes ($>0.003 \text{\AA}$) are highlighted in blue and red, respectively.

Table 6. Calculated^{a)} and Experimental Cone Angles (θ_{cal} and θ_{exp}) of **1**, **3**, and **4**

Position	Cone angle $\theta_{\text{cal}}/^\circ$			Cone angle $\theta_{\text{exp}}/^\circ$	
	1	3	4	1	3
C7	76.72	76.64	76.35	76.83 ^{b)}	76.78
C10	76.72	76.65	76.16	76.83 ^{b)}	76.83
C8	71.33	71.26	70.65	71.82 ^{b)}	71.96
C9	71.33	71.27	70.52	71.82 ^{b)}	72.01
C11	75.06	74.85	73.12	74.67	74.43

a) B3LYP/6-311+G(d,p). b) Average value between θ (C7) and θ (C10) and between θ (C8) and θ (C9), respectively.

Table 7. Differences $\Delta\theta$ between Cone Angles θ_{cal} (B3LYP/6-311+G(d,p)) and θ_{exp} of **1**, **3**, and **4**^{a)}

Position	$\Delta\theta_{\text{cal}}/^\circ$		$\Delta\theta_{\text{exp}}/^\circ$	$\Delta\theta = \theta_{\text{exp}} - \theta_{\text{cal}}/^\circ$	
	$\theta(\mathbf{3}) - \theta(\mathbf{1})$	$\theta(\mathbf{4}) - \theta(\mathbf{3})$	$\theta(\mathbf{3}) - \theta(\mathbf{1})$	1	3
C7	-0.08	-0.29	-0.05	0.11	0.14
C10	-0.07	-0.49	0.00	0.11	0.18
C8	-0.07	-0.61	0.14	0.49	0.70
C9	-0.06	-0.75	0.19	0.49	0.74
C11	-0.21	-1.73	-0.24	-0.39	-0.42

a) Narrower and wider changes are highlighted in blue and red, respectively.

magnitude of the effect is significant at C8, C9, and C11 in both **1** and **3**. However, the differences in depth at C8 and C9 of **3** (-0.042 and -0.044 , respectively) are much bigger than the corresponding values in **1** (-0.028 and -0.028 , respectively). The pronounced effects of intermolecular interactions on the shallowness at C8 and C9 of **3** appear to overwhelm the effects of introducing of the methyl group (0.011 and 0.002 at C8 and C9, respectively, from Δd_{cal} between d_{cal} of **3** and d_{cal} of **1**), resulting in a shallower change Δd_{exp} between **3** and **1** in the crystal (-0.003 and -0.013 , respectively). With regard to the comparison between the value d_{cal} for **4** and that of **3**, the introduction of the carbonyl groups induces markedly deeper bowl depth at every position.

From the analysis of the bowl depth, one can easily obtain a clear picture of the effect on the sumanene skeleton of methyl groups, which increase the depth at every position, as well as the effects of intermolecular interactions in the crystal, which cause an increase in depth at C11 and a reduction in depth at other positions. However, the changes in bond length (Figure 9) are not directly correlated to the changes in bowl depth (Table 5), except that longer bond lengths at C7–C8 and C8–C9 in **2** can increase the calculated bowl depth at C8. Thus, the change in bowl depth is the result of a change in the angle of the bowl shape. Since the POAV angle is not a suitable parameter for identifying changes in the bowl shape, the cone

angle θ (Figure 8) was introduced to identify the critical points for structural changes in the bowl shape. The cone angles θ at C7, C10, C8, C9, and C11 in **1**, **3**, and **4**, and the differences in these angles ($\Delta\theta$) are shown in Tables 6 and 7. We also found a good correlation between the changes in the bowl depth and the changes in the cone angle, as evident from Tables 5 and 7. On the introduction of the methyl groups, the optimized geometries of **1** and **3** exhibited a narrower calculated cone angle θ_{cal} at every position, resulting in a deeper bowl depth. In the crystal of **3**, the angles θ_{exp} at C8 and C9 were narrower and the angle θ_{exp} at C11 was wider than the corresponding angles in **1**. Intermolecular interactions in the crystal therefore result in a narrower cone angle θ_{exp} at C11 and wider cone angles θ_{exp} at other positions, producing the observed changes in bowl depth listed in Table 5. The magnitudes of the changes are consistent with one another.

The observed effects of intermolecular interactions can be interpreted in terms of repulsive and attractive interactions in the crystal packing of **1** and **3** (Figure 10). The repulsive interaction corresponds to intermolecular steric repulsion between the benzene rings and the *exo*-H atoms of the cyclopentadiene rings, which induces a narrower cone angle θ_{exp} at C11 and wider cone angles θ_{exp} at C8 and C9. The attractive interaction corresponds to the CH– π interaction between the benzene rings and the *endo*-H atoms of the cyclopentadiene

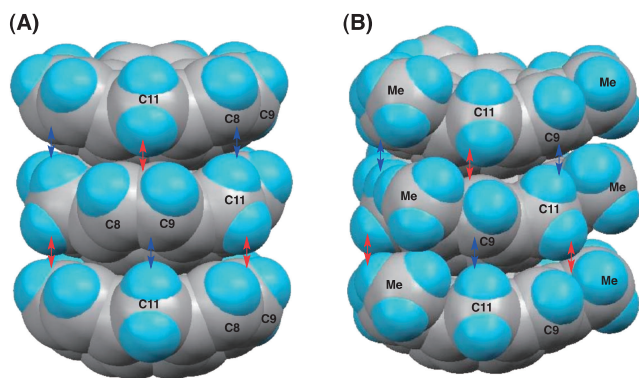


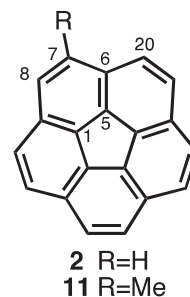
Figure 10. Repulsive (red) and attractive (blue) interactions of (A) **1** and (B) **3** in the crystal packing.

rings, as discussed in the previous section (Figure 7). The combination of repulsive and attractive interactions induces the observed structural changes in **1** and **3** (Figure 10). The repulsive interaction appears to be enhanced by the steric hindrance of the methyl group, which results in a bigger change in angle θ_{exp} at C8 and C9 in **3** than in **1**.

Substituent Effects: Sumanene versus Corannulene. A comparative analysis of several parameters for trimethylsumanene (**3**) with those of sumanene (**1**) showed that the introduction of methyl groups causes the cone angle of the bowl shape to be narrower and the bowl depths to be deeper, in addition to producing an increase in the lengths of the C7–C8 and C8–C9 bonds in sumanene. This finding is surprising, because Siegel and co-workers reported that the bowl shape of corannulene (**2**) becomes shallower on the introduction of substituents.¹¹ To compare the two molecules, we calculated the optimized bowl structures of corannulene (**2**) and methylcorannulene (**11**) at the B3LYP/6-311+G(d,p) level of theory. Selected structural parameters for **2** and **11** and the differences between them are shown in Table 8. The C6–C7 and C7–C8 bonds in **11** are longer than the corresponding bond in **2**, in a similar manner to the case of trimethylsumanene (**3**). However, the bowl depth is shallower and the cone angle is wider in the methylated derivative, in contrast to the case of sumanene. Similar structural changes have been reported for corannulene substituted with various other groups. The effect of these substituents has been explained by an increase in steric repulsion through *peri* interactions of the substituents. In general, the direction of the structural change to a deeper or shallower bowl depth is governed by two factors: steric repulsion and electronic effects. To elucidate the difference between sumanene and corannulene, we made a thorough analysis of these two factors.

First, we compared the electronic effects of the methyl group on sumanene and corannulene. The electronic effect of the substituent stabilizes the core structure through conjugation between the substituent and the core structure. The bowl shape is governed by the difference in the stabilization effect between the bowl structure and the flat structure corresponding to the transition state for the bowl inversion. We assumed that the electronic stabilization effect is bigger in the flat structure than in the bowl structure, because the conjugation is maximized by overlapping of orbitals in the flat structure. Indeed, an NBO

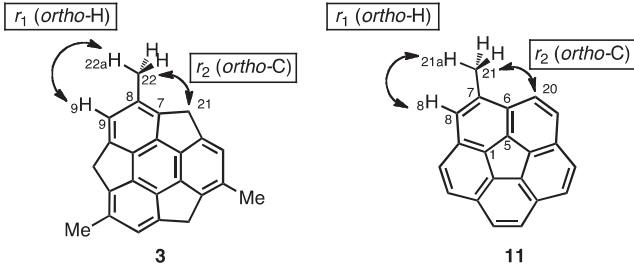
Table 8. Calculated (B3LYP/6-311+G(d,p)) Structural Parameters for Corannulene (**2**) and Its Methylated Derivative **11**, and Differences between the Two Compounds



Parameter	Position	2	11	Difference
				(11) – (2)
Bond length/Å	r (C6–C7)	1.446	1.458	0.012
	r (C7–C8)	1.386	1.390	0.004
Bowl depth/Å	d (C7)	0.889	0.883	–0.006
	d (C8)	0.889	0.879	–0.010
Cone angle/°	θ (C7)	74.73	74.78	0.05
	θ (C8)	74.73	74.86	0.13

analysis of the calculated flat and bowl structures of methylsumanene and methylcorannulene (B3LYP/6-311+G(d,p)) showed that the flat structure is stabilized to a greater degree in both sumanene (0.33 kcal mol^{–1}) and corannulene (0.50 kcal mol^{–1}). Thus, the electronic effect of the methyl group leads to a shallower structure, which is consistent with the observed structural change of methylcorannulene (**11**) but not that of trimethylsumanene (**3**).

Next, we analyzed the difference in the steric effects of methyl groups in sumanene and corannulene. In the optimized bowl and flat structures of both **3** and **11** (B3LYP/6-311+G(d,p)), one hydrogen atom of the methyl group is oriented toward the *ortho*-hydrogen of the ring structure, as shown in Table 9. The major steric repulsions are those between the hydrogen of the methyl group and the *ortho*-hydrogen (H_{22a} and H₉ in sumanene; H_{21a} and H₈ in corannulene) and between the carbon of the methyl group and the *ortho*-carbon (C₂₂ and C₂₁ in sumanene, C₂₁ and C₂₀ in corannulene). Their distances (r_1 (*ortho*-H), r_2 (*ortho*-C)) and the differences (Δr_1 , Δr_2) from van der Waals radii (r_0) are shown in Table 9.¹⁹ In both sumanene and corannulene, the distance (r_1 (*ortho*-H)) between the methyl hydrogen and the *ortho*-hydrogen is shorter in the flat structure than in the bowl structure, and is within the van der Waals radius ($\Delta r_1 < 0$), whereas the distance (r_2 (*ortho*-C)) between the methyl carbon and the *ortho*-carbon is shorter in the bowl structure than in the flat structure within the van der Waals radius ($\Delta r_2 < 0$). Thus, steric repulsion against the *ortho*-hydrogen is increased in the flat structures, thereby favoring a deeper bowl structure. On the other hand, steric repulsion against the *ortho*-carbon is increased in the bowl structure, tending to favor a shallower bowl structure. This means that the direction of the structural change is determined by the balance between these two opposing steric effects. In the case of **3**, steric repulsion of the *ortho*-hydrogen has a greater effect than that of the *ortho*-carbon because of the wider bay angle (C8–C7–C21) arising from the fusion of the six- and five-

Table 9. Steric Repulsions in Calculated (B3LYP/6-311+G(d,p)) Trimethylsumanene (**3**) and Methylcorannulene (**11**) and the Internuclear Distances in These Compounds


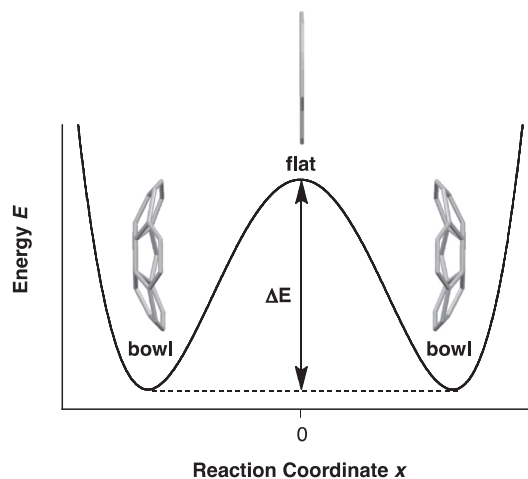
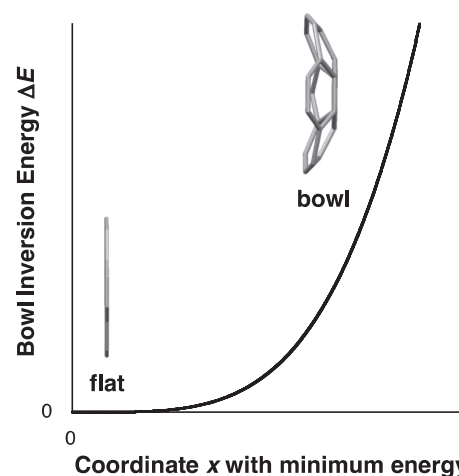
Position	3		11	
	Bowl	Flat	Bowl	Flat
$r_1(\text{ortho-H})^a$	2.335	2.268	2.310	2.287
$r_2(\text{ortho-C})^a$	3.292	3.509	3.154	3.298
$\Delta r_1 = r_1 - r_0(\text{H-H})^b$	-0.065	-0.132	-0.090	-0.113
$\Delta r_2 = r_2 - r_0(\text{C-C})^b$	-0.108	0.109	-0.246	-0.102

a) $r_1(\text{ortho-H})$: distance between H22a and H9 in **3** or H21a and H8 in **11**; $r_2(\text{ortho-C})$: distance between C22 and C21 in **3** or C21 and C20 in **11**. b) $r_0(\text{H-H})$, $r_0(\text{C-C})$ are, respectively, the H-H and C-C distances calculated from the van der Waals radii with H = 1.20 Å and C = 1.70 Å.¹⁹ Δr_1 and Δr_2 are, respectively, the difference between $r_1(\text{ortho-H})$ and $r_0(\text{H-H})$ or between $r_2(\text{ortho-C})$ and $r_0(\text{C-C})$. Between the value (r or Δr) of the bowl structure and that of the flat structure, shorter r and more negative Δr are highlighted by colors, where blue color or red color favors shallower bowl or deeper bowl, respectively. The values shown in boldface result in more significant steric repulsions between the blue and red values.

membered rings. Thus, the steric effect of the methyl group in sumanene results in a deeper bowl structure. In contrast, the steric repulsion of the *ortho*-carbon in methylcorannulene (**11**) is more significant, owing to the narrower bay angle (C7–C6–C20) of the fully six-membered-ring structure. The steric effect of the methyl group therefore favors a shallower bowl structure in corannulene.

The cooperative electronic and steric effects of a methyl substitute thus favor a shallower bowl structure in corannulene. The shallower structural change in methylcorannulene (**11**) is consistent with the lower bowl-inversion energy of **11**. In the case of sumanene, although the two effects of the methyl group are in opposition to one another, the steric effect is greater than the electronic effect, leading to a deeper bowl structure on introduction of methyl substituents. The structural changes in **3** are matched by a higher bowl-inversion-energy change.

Structure–Bowl-Inversion Energy Correlation. Siegel and co-workers investigated bowl depths and bowl-inversion energies of many substituted corannulenes.¹¹ From their experimental and calculated results, they proposed a correlation between the bowl depth and the inversion energy of corannulenes in the form of a double-well potential equation $E = ax^4 - bx^2$, where E is the energy, x is the reaction coordinate (bowl depth), and a and b are coefficients (Figure 11). The bowl-inversion energy ΔE is given by the equation $\Delta E = E_0 - E_1 = ax_1^4$, where E_0 is the energy for the flat structure corresponding to the transition state for the bowl

**Figure 11.** Double-well potential model $E = ax^4 - bx^2$ of bowl inversion for the sumanene structure. a , b : coefficients, ΔE : bowl-inversion energy.**Figure 12.** Correlation between the structure and the bowl-inversion energy for a double-well potential model $\Delta E = ax^4$ with the sumanene structure. a : coefficient.

inversion and E_1 and x_1 are the energy and reaction coordinate, respectively, for a bowl structure with a minimum energy (Figure 12). The experimental and calculated values for corannulenes are well fitted by this model. Corannulene tends to adopt a shallower bowl depth and a lower bowl-inversion energy on the introduction of substituents other than cyclic substituents. With the experimental and calculated bowl structures and bowl-inversion energies of sumanene (**1**), trimethylsumanene (**3**), and trimethylsumanenetrione (**4**) in hand, we analyzed their correlation by the double-well potential model $E = ax^4 - bx^2$ and $\Delta E = ax^4$ (Figures 11 and 12, respectively). For this analysis, we selected the cosine of the cone angle θ as the reaction coordinate x , and we used three cone angles independently (the average at C8 and C9 (C8–C9), the average at C7 and C10 (C7–C10), and angle at C11). Plots of the calculated $\cos \theta_{\text{cal}}$ at (A) C8–C9, (B) C7–C10, and (C) C11, and the experimental ΔE_{exp} for compounds **1**, **3**, and **4** are shown in Figure 13, as well as the plots of the calculated $\cos \theta_{\text{cal}}$ and ΔE_{cal} , and the experimental $\cos \theta_{\text{exp}}$ and ΔE_{exp} . At the energy-minimum point, the coefficients a and b are given by the

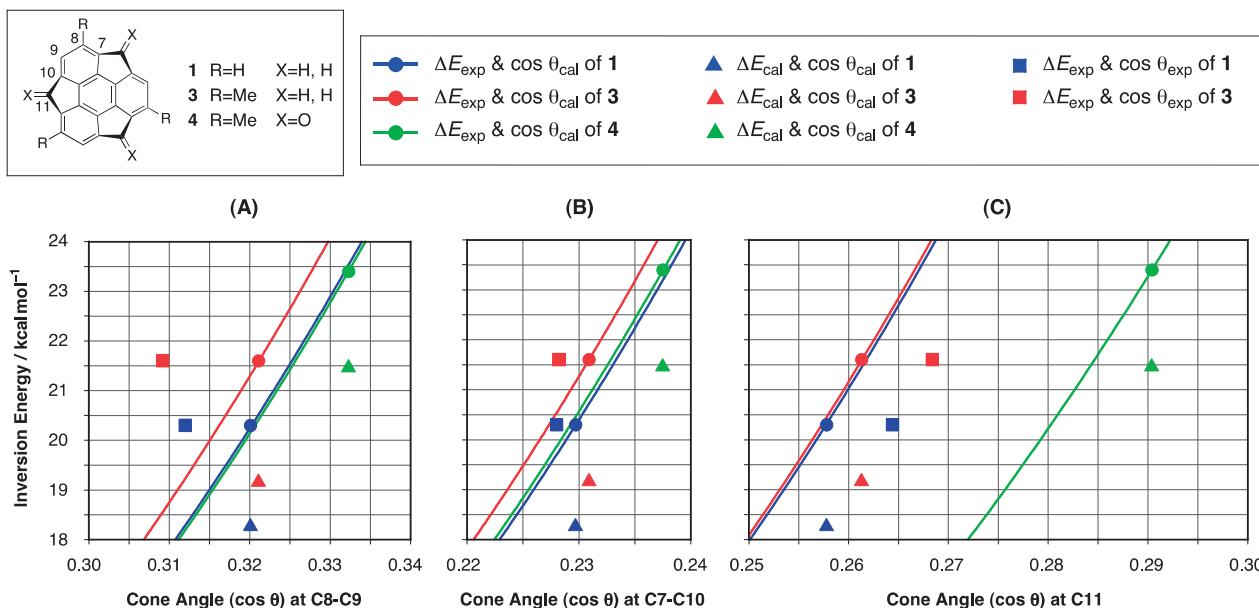


Figure 13. Plot of the cone angle ($\cos \theta$) against the bowl-inversion energy (ΔE). (A) Average θ at C8 and C9, (B) average θ at C7 and C10, (C) θ at C11. Circle dot: calcd $\cos \theta_{\text{cal}}$ (B3LYP/6-311+G(d,p)), exptl ΔE_{exp} with $\Delta E = a \cos^4 \theta$ curve; triangle dot: calcd $\cos \theta_{\text{cal}}$, calcd ΔE_{cal} ; square dot: exptl $\cos \theta_{\text{exp}}$, exptl ΔE_{exp} , of sumanene (**1**) (blue), trimethylsumanene (**3**) (red), and trimethylsumanenetrone (**4**) (green).

Table 10. Coefficients a and b from the Experimental Bowl-Inversion Energy ΔE_{exp} and the Calculated^{a)} Cone Angle ($\cos \theta_{\text{cal}}$) at (A) C8–C9, (B) C7–C10, and (C) C11

Position ^{b)}	Coefficient ^{c)}	1	3	4
(A) C8–C9	a	1.93	2.03	1.92
	b	3.96	4.19	4.24
(B) C7–C10	a	7.29	7.60	7.35
	b	3.96	4.19	8.30
(C) C11	a	4.60	4.63	3.29
	b	6.11	6.32	5.55

a) B3LYP/6-311+G(d,p). b) C8–C9: average at C8 and C9, C7–C10: average at C7 and C10. c) a : $\times 10^3$; b : $\times 10^2$.

equations $a = \Delta E/x^4$, $b = 2ax^2$, respectively. By using the calculated $\cos \theta_{\text{cal}}$ and the experimental ΔE_{exp} for **1**, **3**, and **4**, the coefficients a and b were determined as listed in Table 10, and the curve for $\Delta E = a \cos^4 \theta$ is shown in Figure 13.

The difference between the calculated value ΔE_{cal} and the experimental value ΔE_{exp} shows that ΔE_{cal} for **1**, **3**, and **4** is underestimated with almost similar degree (1.9–2.4 kcal mol⁻¹) (Figure 13; see also Table 1). As already discussed, the experimental cone angles θ of **1** and **3** show some differences owing to intermolecular interactions in the crystal (Figure 13; see also Tables 6 and 7). At C8 and C9, the experimental values of $\cos \theta_{\text{exp}}$ for **1** and **3** are significantly shifted to smaller values in comparison with the calculated value $\cos \theta_{\text{cal}}$. Because the magnitude of the change in **3** is much greater than that in **1**, the experimental value $\cos \theta_{\text{exp}}$ of **3** is smaller than $\cos \theta_{\text{exp}}$ for **1**, whereas the calculated value $\cos \theta_{\text{cal}}$ for **3** is bigger than $\cos \theta_{\text{cal}}$ for **1**. On the other hand, the shift at C7 and C10 is small and of a similar magnitude in both **1** and **3**. Thus, the experimental values $\cos \theta_{\text{exp}}$ at C7 and C10 show a better fit to the calculated values $\cos \theta_{\text{cal}}$. At C11, the experimental value

of $\cos \theta_{\text{exp}}$ for both **1** and **3** are significantly enlarged. However, the order for **1** and **3** is not different from that of the calculated $\cos \theta_{\text{cal}}$, because the magnitudes of the shifts in **1** and **3** are similar. This analysis suggests that the calculated value of $\cos \theta_{\text{cal}}$ at C7–C10 can be supported by a comparison with the experimental value $\cos \theta_{\text{exp}}$ in the crystal in discussing the structure–bowl-inversion energy correlation, because these cone angles are less affected by intermolecular interactions in the crystal.

Coefficients a of **1** and **3** show good fits to one another at every position with small deviations (Figure 13 and Table 10). In detail, there are small deviations at C8–C9 and C7–C10, whereas there is almost no deviation at C11. In general, a deviation in coefficient a is caused by a deviation in the reaction coordinate (structure) and/or a deviation in the bowl-inversion energy from the values predicted by the original $E = ax^4 - bx^2$ equation. A deviation in the structure arises from a partial change in structure caused by the presence of a substituent. The deviation in bowl-inversion energy is caused by a significant difference in the electronic stabilization effects between the bowl structure and the flat structure. Because, in the case of **3**, a small deviation is observed at C8–C9 and C7–C10, but not at C11, the deviation of coefficient a for **3** arises mainly from a deviation in the reaction coordinate resulting from the small structural deviations at C8–C9 and at C7–C10. If the deviation in the bowl-inversion energy had the greater influence, deviations of a similar magnitude would be observed at all positions.

Coefficient b determines the reaction coordinate with a minimum energy on the $\Delta E = ax^4$ curve. Because the deviation of coefficient a for **3** from that of **1** is relatively small, coefficient b is more responsible for the difference between **1** and **3**. The steric repulsion between the methyl group and the *ortho*-hydrogen destabilized the flat structure more than the

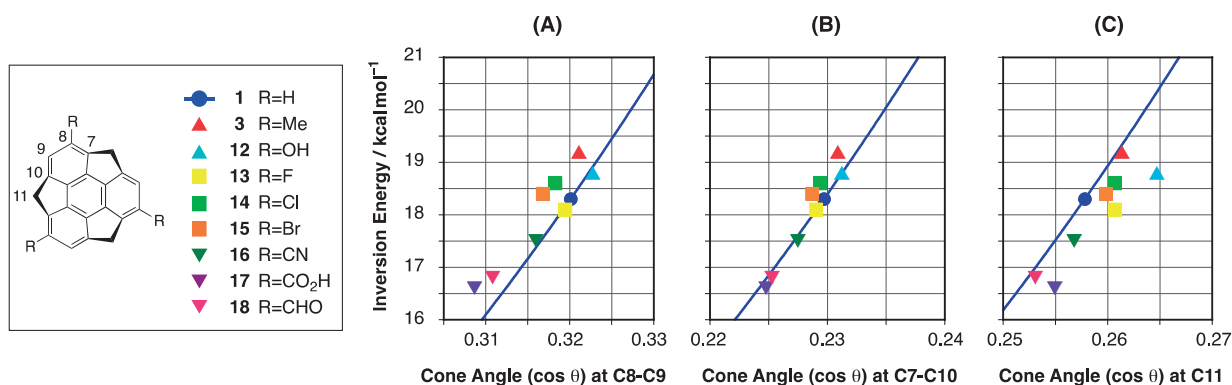


Figure 14. Plot of the calculated cone angle ($\cos \theta_{\text{cal}}$) versus the bowl-inversion energy (ΔE) of trisubstituted sumanenes (B3LYP/6-311+G(d,p)), together with the $\Delta E = a \cos^4 \theta$ curve of **1** (blue line). (A) Average θ at C8 and C9, (B) average θ at C7 and C10, (C) θ at C11.

bowl structure, which leads to a deeper bowl and a higher value of ΔE .

In contrast to the difference between **1** and **3**, the coefficient a for **4** is smaller at every position than the corresponding value for **3**. Whereas the deviations of coefficient a at C8–C9 and C7–C10 are small, that at C11 is quite large. The significant deviation at C11 reflects the significant change in $\cos \theta$ at C11 caused by the marked structural change from sp^3 to sp^2 hybridization at this position. From a different point of view, the good fit between the $\Delta E = a \cos^4 \theta$ curves at C8–C9 and C7–C10 for **4** with those of **1** and **3** is surprising, in that the marked structural change at C11 does not appear to induce a large deviation at these positions. Furthermore, the sumanene derivatives **3** and **4**, which are substituted at different positions, can still share the $\Delta E = a \cos^4 \theta$ curve for **1** at C8–C9 or C7–C10 with little deviation.

The thorough analysis of the structure–bowl inversion correlation for **1**, **3**, and **4** based on the $E = ax^4 - bx^2$ equation suggests a suitable reaction coordinate for structure–energy correlation analysis with a unified equation. The reaction coordinate close to an introduced substituent is affected to a greater degree by the structural deviation, causing a significant deviation from the original $\Delta E = ax^4$ equation. A reaction coordinate distant from the introduced substituent is more suitable, because of the minimal deviation from the original $\Delta E = ax^4$ equation. In the case of substituted sumanenes, an analysis at C7–C10 is favorable in this sense.

After our thorough analysis of **1**, **3**, and **4**, our next aim was to focus on the effects of other substituents on the structure and the bowl-inversion energy. Siegel and co-workers investigated the bowl structure and bowl-inversion energy of corannulenes with various substituents and substitution patterns,¹¹ and they reported that acyclic substituents lead to a shallower bowl and to a lower bowl-inversion energy in corannulene. However, the effects of individual substituents were not clear in their study because of mixing of various substituents and substitution patterns. Because the reliability of the B3LYP/6-311+G(d,p) method for calculating the structure and bowl-inversion energy was well demonstrated in the cases of **1** and **3**, we continued to use this method to predict the substituent effects and structure–bowl inversion energy correlations for the C_3 symmetric sumanenes **12–18** containing other substituents (Figure 14).

Figure 14 shows plots of the calculated cone angles ($\cos \theta_{\text{cal}}$) at C8–C9, C7–C10, and C11 and of the calculated bowl-inversion energies ΔE_{cal} for **1**, **3**, and **12–18**, together with the $\Delta E = a \cos^4 \theta$ curve of **1**. Interestingly, the substituent effect varies with the nature of the substituent, affording deeper or shallower bowl structures and higher or lower bowl inversion energies. At every position, the plots for compounds **12–18** show a good fit with the $\Delta E = a \cos^4 \theta$ curve of **1**. Trihydroxysumanene (**12**) is predicted to possess a bigger $\cos \theta_{\text{cal}}$ and a higher ΔE_{cal} than **1** or **3**. Trihalosumanenes **13**, **14**, and **15** show similar values of $\cos \theta_{\text{cal}}$ and ΔE_{cal} to **1**. **16** with cyano groups, **17** with carboxy groups, and **18** with formyl groups show a smaller value of $\cos \theta_{\text{cal}}$ and a lower value of ΔE_{cal} than **1**. These substituent effects on the structure and on the bowl-inversion energy can be explained in terms of a combination of electronic and steric effects of the substituents. Trihydroxysumanene (**12**) shows a shortened distance (r_1 (*ortho*-H)) between the hydroxy group and the *ortho*-hydrogen in the flat structure, in a similar manner to **3** (Figure 15 and Table 11), leading to a deeper bowl and a higher value of ΔE . Halogens of **13**, **14**, and **15** do not induce significant differences between the steric repulsions in the bowl structures and those in the flat structures. Although the cyano group of **16** does not induce a significant difference in steric repulsion, the flat structure is stabilized to a greater degree by electronic effects through π -conjugation, leading to a shallower bowl and a lower ΔE . The optimized bowl and flat structures of **17** show that the direction of carboxy group is opposite in the bowl and the flat structures (Figure 15 and Table 11). Nevertheless, the flat structure is considered to be more stabilized by the electronic effect through the π -conjugation, in a similar manner to **16**, leading to a shallower bowl and a lower ΔE . In contrast, the steric effect causes an opposite effect to that in **3** or **12**, because of the rotation. Unlike **3** or **12**, the distance to *ortho*-hydrogen (r_1 (*ortho*-H)) is shortened in the bowl structure compared with the flat structure because the angle C8–C22–O22a is wider than the angle C8–C22–O22b. Thus, the steric repulsion against the *ortho*-hydrogen is increased in the bowl structure. The steric repulsion against the *ortho*-carbon (r_2 (*ortho*-C)) is increased in the bowl structure owing to the shorter distance, in a similar manner to that in **3** or **12**. As a result, both steric repulsions lead to a shallower bowl. The cooperative electronic and steric effects result in a shallower

bowl and a lower ΔE , even compared with **16**. In the case of **18**, the electronic effects of formyl groups lead to a shallower bowl and a lower ΔE . In contrast, the steric effects seem to cause a deeper bowl and a higher value of ΔE because of the shortened distance (r_1 (*ortho*-H)) between the formyl group and the *ortho*-hydrogen in the flat structure in a similar manner to **3** and **12** (Figure 15 and Table 11). In spite of the conflicting

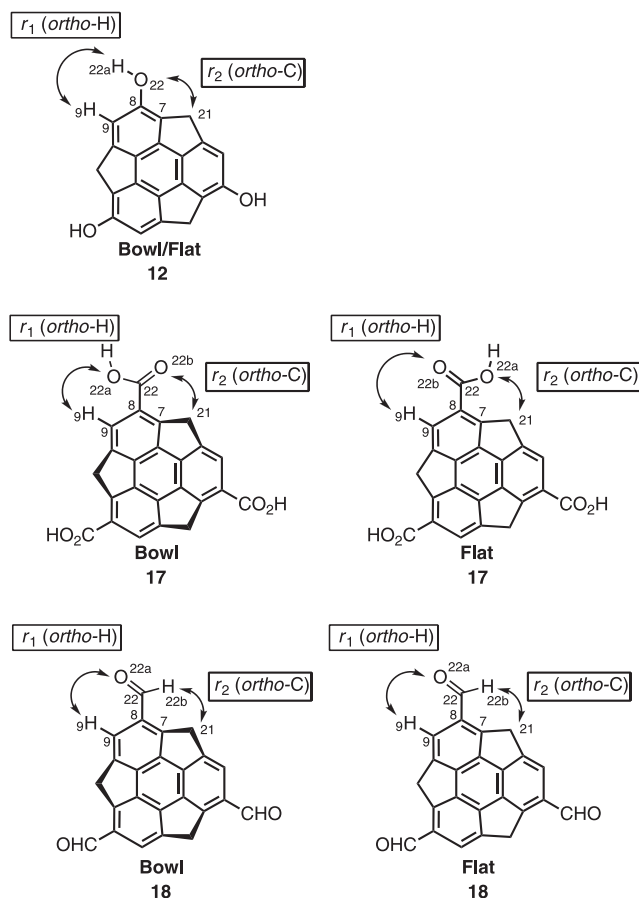


Figure 15. Interactions of peripheral atoms cause steric repulsion in the calculated structures (B3LYP/6-311+G(d,p)).

steric and electronic effects, **18** shows a much shallower bowl and a lower ΔE (Figure 14). Although the quantitative analysis of the magnitude of the steric and electronic effects is difficult at this point, a possible explanation is that the stronger electronic effects overwhelm the weaker steric effects. The relatively smaller difference between the Δr_1 (-0.210) at the bowl structure and that (-0.236) at the flat structure (Table 11), compared with those of **3** and **12**, could support the weaker steric effects leading to deeper bowl structure.

From this analysis, we can conclude that the substituent effect on the bowl structure and the inversion energy vary depending on the nature of the substituent. The structure–bowl–inversion energy correlation of sumanenes with a variety of substituents can be fitted to a double-well potential model with a unified equation. The effects of the substituents can be explained in terms of a combination of their electronic and steric effects, with the conformation of the substituents playing an important role.

Columnar Crystal Packing and Electron Conductivity.

As mentioned in the section of crystal packing of trimethylsumanene (**3**), the molecular-packing structures of crystalline buckybowl are classified into three types; (A) columnar convex-to-concave stacks with all columns in a constant direction, (B) columnar convex-to-concave stacks with neighboring columns in opposite directions, and (C) noncolumnar structures (Figure 4). Although the difference of packing structure must be strongly correlated to the electronic properties, the correlations have not been studied until now. Sumanene (**1**) possesses a columnar packing structure with unidirectional columns of type A,^{6a} and it has been reported to possess a high electron mobility ($0.75 \text{ cm}^2 \text{ V}^{-1} \text{ s}^{-1}$) and a large anisotropy (9.2 times) along the columnar axis, as measured by the TRMC method.^{6d} Trimethylsumanene (**3**) has a similar columnar packing structure to **1**, but with neighboring columns oriented in opposite directions, and is therefore of type B. Sumanenes **1** and **3** are therefore ideal examples for studying the effects of the column alignment on the electron-transport properties, especially the effects on the anisotropic mobility of electrons of ratchet-type potentials along the stacking axes.

The charge carrier mobility in **1** and **3** were also examined by means of electrodeless TRMC measurements in the present

Table 11. Nuclear Distances to Cause Steric Repulsion in the Calculated Structures (B3LYP/6-311+G(d,p))

Position	12		17		18	
	Bowl	Flat	Bowl	Flat	Bowl	Flat
$r_1(\textit{ortho}\text{-H})^{\text{a}}$	2.227	2.178	2.353	2.435	2.510	2.484
$r_2(\textit{ortho}\text{-C})^{\text{a}}$	3.143	3.377	3.010	3.072	2.890	3.092
$\Delta r_1 = r_1 - r_0(\text{X-H})^{\text{b}}$	-0.173	-0.222	-0.367	-0.285	-0.210	-0.236
$\Delta r_2 = r_2 - r_0(\text{Y-C})^{\text{b}}$	-0.077	0.157	-0.210	-0.148	-0.010	0.192

a) r_1 : distance between H22a and H9 in **12**, O22a and H9 in bowl-**17** and **18**, O22b and H9 in flat-**17**; r_2 : distance between O22 and C21 in **12**, O22b and C21 in bowl-**17**, O22a and C21 in flat-**17**, H22b and C21 in **18**. b) $r_0(\text{X-H})$ and $r_0(\text{Y-C})$ are, respectively, the H–H (X = H) and O–C (Y = O) distances for **12**, the O–H (X = O) and O–C (Y = O) distances for **17**, and the O–H (X = O) and H–C (Y = H) distances for **18** calculated from the van der Waals radii with H = 1.20 Å, C = 1.70 Å, O = 1.52 Å.¹⁹ Δr_1 and Δr_2 are, respectively, the difference between $r_1(\textit{ortho}\text{-H})$ and $r_0(\text{X-H})$ or between $r_2(\textit{ortho}\text{-C})$ and $r_0(\text{Y-C})$. Between the value (r or Δr) of the bowl structure and that of the flat structure, shorter r and more negative Δr are highlighted by colors, where blue color or red color favors shallower bowl or deeper bowl, respectively. The values shown in boldface result in more significant steric repulsions between the blue and red values.

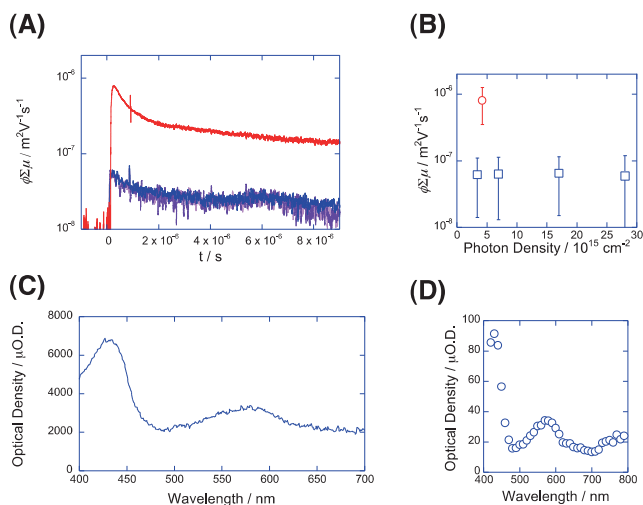


Figure 16. (A) Observed conductivity transients in compounds **1** (red) and **3** (blue-violet). The transients were recorded at room temperature with excitation at 355 nm at a photon density of 3.5×10^{15} (red and violet) to 2.8×10^{16} photons cm^{-2} (blue). (B) Plot of the maximum values of conductivity against the excitation photon density. (C) Transient absorption spectrum of a polycrystalline film of **3** (average thickness 2.5 μm) with excitation at 355 nm by 9×10^{16} photons cm^{-2} . The spectrum was recorded 5 μs after the pulse exposure. (D) Transient absorption spectrum of radical anions of **3**, recorded at 100 ns after irradiation of a 30 mM solution of **3** in methyltetrahydrofuran by a 130-Gy electron pulse. The solution (10 cm^3) was deaerated by bubbling argon gas for 10 min before recording the spectra.

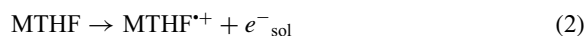
study. Figure 16A shows the conductivity transients observed for polycrystalline samples of both **1** and **3** upon excitation by Nd:YAG laser pulses (FWHM \approx 6 ns) at 355 nm. The observed values of maximum conductivity are also plotted against the excitation photon density in Figure 16B. The kinetic traces for **3** in Figure 16A overlap in the range of excitation photon density from 3.5×10^{15} to 28×10^{15} photons cm^{-2} . In an unsubstituted sumanene single crystal, second-order kinetics play a crucial role in the recombination processes of photo-generated electrons and holes in an isolated column of sumanene with π -stacking,^{6d} however, unlike the case of **1**, the trimethyl derivative **3** shows relatively little contribution from second-order recombination processes. This view is also supported by the almost constant values of $\phi \sum \mu$, as shown in Figure 16B.

The conductivity ($\Delta\sigma$) was determined from the transient microwave absorption in the TRMC measurements, and is given as a function of the changes in the reflected microwave power ($\Delta P/P_r$) from a microwave cavity containing the sample;

$$\Delta\sigma = e\phi N \sum \mu = \frac{1}{A} \frac{\Delta P_r}{P_r} \quad (1)$$

where A is a sensitivity factor, e is the elementary charge on the electron, ϕ is the quantum efficiency for photocarrier generation, N is the number of photons absorbed by the samples, and $\sum \mu$ is the sum of the mobilities for negative and positive

carriers.²⁰ The value of ϕ is essential for determining the value of the mobility. The transient optical absorption spectra were recorded with identical polycrystalline films. Figure 16C shows the transient optical absorption spectrum of **3**, in which two distinct absorption bands are observed at about 430 and 580 nm, respectively. To assign these absorption bands, the spectrum of the radical anion of **3** was also recorded by a radiolytic method in a solution, as shown in Figure 16D. The spectrum was measured in a solution of **3** in methyltetrahydrofuran (MTHF), where the following radiolytic reaction occurs:²¹



From the radiolytic dose applied to the system and the rate constant for the reaction of the solvated electron (e^-_{sol}) with **3**, the yield of negative ion was estimated quantitatively at the time the spectrum was recorded to give the molar extinction coefficient of the **3** radical anion ($\mathbf{3}^{\bullet-}$) as $\epsilon^- = 2.4 \times 10^4$ $\text{mol}^{-1} \text{dm}^3 \text{cm}^{-1}$ (at 430 nm).²²

The transient absorption spectrum observed under photoexcitation (Figure 16C) is almost identical to that shown in Figure 16D; the radical anions of **3** are therefore the major intermediates present 5 μs after exposure to the UV pulse. This also suggests that the major charge carriers are electrons on **3**. The value of ϵ^- gives an estimate of ϕ as ≈ 0.003 from the photoexcitation spectrum, leading to a mobility in **3** of $\mu = 0.2 \text{ cm}^2 \text{V}^{-1} \text{s}^{-1}$. Anisotropic mobility value of $0.75 \text{ cm}^2 \text{V}^{-1} \text{s}^{-1}$ in a sumanene single crystal leads to the isotropic value of $0.25 \text{ cm}^2 \text{V}^{-1} \text{s}^{-1}$ with an assumption of the random orientation of the crystallographic axes of the polycrystalline state, suggesting striking agreement to the values in the present case. On the basis of the crystallographic analysis of **1** and **3**, differences in the respective stacking distances ($\Delta d < 0.1 \text{ \AA}$) and the rotation angles ($\Delta\theta$) are minimal, leading to equivalent local motion of the electrons along the stacking axes in the present case. Derived value of the anisotropic electron mobility; $\mu \approx 0.6 \text{ cm}^2 \text{V}^{-1} \text{s}^{-1}$ also gives the estimated spatial size of the local motion of carriers as 15 nm from the turnover period of microwave (110 ps), Q value of the microwave cavity ($Q = 2500$), and the electric field strength $E \approx 10^1 \text{ V cm}^{-1}$. This is suggestive that the electron-hole pairs lead respective free charge carriers when the negative and positive charges are apart at the interval longer than few tens nm. The yield of photocarrier generation was markedly less in **3** ($\phi \approx 0.003$) than in **1** ($\phi \approx 0.06$).^{6d} The unidirectional columnar packing in **1** produces a ratchet-type potential along the stacking axes, which leads to asymmetric potential barriers for transport of electrons and holes along the axes. This may be the cause of the 20-fold higher value of ϕ in **1** upon excitation at 355 nm and it also suggests that the unique stacking structure of the present buckybowl systems leads to unique anisotropic photoelectric properties when they are in their crystalline state.

Summary

We have developed a selective and direct approach for the synthesis of C_3 symmetric trisubstituted sumanenes from C_3 symmetric functionalized *syn*-tris(norborneno)benzene precursor. By using an enantiopure precursor with an sp^3 stereogenic

center and by realizing chiral transmission to bowl chirality at low temperatures, we achieved the first enantioselective synthesis of the chiral C_3 symmetric buckybowl trimethylsumanene (**3**). Bowl inversion, corresponding to racemization of the chiral buckybowl, was frozen by the introduction of substituents to generate sp^3 stereogenic centers or controlled by functionalization to increase the bowl inversion energy; this permitted chiral HPLC to be used to analyze and to resolve trimethyltris(trimethylsilyl)sumanene (**10**) and trimethylsumanenetrione (**4**). The bowl-inversion energies of **3** and **4** were determined by means of time-dependent CD spectral measurements on the enantiomerically enriched samples of **3** and **4**. This strategy, by the introduction of other substituents and further derivatization, could permit a versatile synthesis of a range of C_3 symmetric substituted sumanenes for elucidation of their physical properties. The resulting chiral buckybawls can also be used in studies on asymmetric molecular recognition through bowl chirality, as well to control the chirality of fullerenes or carbon nanotubes.

We found that **3** has a columnar crystal packing structure in which (*A*)-**3** and (*C*)-**3** are stacked alternately in a convex-to-concave fashion with 46.8° twist angle and with neighboring columns oriented in opposite directions. Theoretical calculations indicate that an attractive interaction derived from an electrostatic interaction or from CH- π interaction plays an important role in favoring this type of stacking.

A detailed structural analysis of sumanene (**1**) and its trimethyl derivative **3**, based on the calculated and experimental data, revealed that the presence of the methyl group results in a deeper bowl, as well as having an effect on the intermolecular interactions in the columnar crystal packing. The difference of the effect of methyl group between sumanene and corannulene was thoroughly investigated in terms of both electronic and steric effects, and it was found that a difference in steric repulsion is responsible for the difference in structure. The double-well potential model was fitted to a bowl structure-inversion energy correlation for **1**, **3**, and the corresponding trione **4**, with a small deviation. A suitable reaction coordinate was identified for analyzing the correlation with a unified equation. The effects of other substituents on the structure and bowl-inversion energy of sumanene were predicted by means of a reliable calculation method. The effects of substituents on the depth of the bowl and the inversion energy can be explained in terms of a combination of electronic and steric effects, if the conformation of the substituents is taken into account. The knowledge on the substituent effects obtained in this study is useful to control a bowl shape and/or a bowl inversion of a buckybowl.

The electron-transport properties of **3** with a bidirectional columnar crystal packing was examined by the TRMC method, and compared with those of **1**, which has a unidirectional columnar packing. Crystals of **3** exhibit an electron mobility ($0.2 \text{ cm}^2 \text{ V}^{-1} \text{ s}^{-1}$) that is equivalent to that of **1**. However, the yield of photocarrier was markedly lower in **3** ($\phi \approx 0.003$) than in **1** ($\phi \approx 0.06$), possibly because the unidirectional columnar packing in **1** produces a ratchet-type potential along the stacking axes and hence an asymmetric potential barrier for transport of electrons and holes along these axes. We also suggest that the unique stacking structure of the present

buckybowl systems leads to unique anisotropic photoelectric properties when the substances are in a crystalline phase. Directional control of the anisotropic transport of electrons in the columnar structures might be realized by design of the molecular stacking to allow for convex-to-concave bowl inversion in the solid state.

Experimental

Single X-ray Crystallographic Analysis. The single-crystal X-ray crystallographic analysis of (\pm)-trimethylsumanene (**3**) was performed on a Rigaku Mercury-CCD (Mo $K\alpha$, $\lambda = 0.71070 \text{ \AA}$, $T = 173 \text{ K}$, $2\theta_{\text{max}} = 55.0^\circ$). Data were collected and processed by using CrystalClear software (Rigaku).²³ The structure was solved by direct methods (SIR2008²⁴) and expanded by Fourier techniques. Refinements were performed by the full-matrix least-squares methods. Hydrogen atoms of methyl groups were calculated and refined as riding atoms. All calculations were performed using the CrystalStructure software package (Rigaku).²⁵

Crystallographic data for (\pm)-**3**: $C_{24}H_{18}$, brown block crystal, $0.05 \times 0.02 \times 0.01 \text{ mm}^3$, monoclinic, space group $P2_1/a$ (No. 14), $a = 7.905(6)$, $b = 17.708(12)$, $c = 11.434(9) \text{ \AA}$, $\beta = 104.010(9)^\circ$, $V = 1553.0(19) \text{ \AA}^3$, $\rho_{\text{calcd}} = 1.310 \text{ g cm}^{-3}$, $Z = 4$, $R_1 = 0.0570$, and $wR_2 = 0.1506$ for 2518 reflections [$I > 2\sigma(I)$], 253 refined parameters.

Crystallographic data have been deposited with Cambridge Crystallographic Data Centre: Deposition number CCDC-850477. Copies of the data can be obtained free of charge via <http://www.ccdc.cam.ac.uk/conts/retrieving.html> (or from the Cambridge Crystallographic Data Centre, 12, Union Road, Cambridge, CB2 1EZ, U.K.; Fax: +44 1223 336033; e-mail: deposit@ccdc.cam.ac.uk).

Computational Methodology. All the theoretical calculations were performed by using the Gaussian 03 or 09 program package.²⁶ The CD spectra of (*C*)-**3** and (*C*)-(8*R*,13*R*,18*R*)-**10** were calculated by TD-DFT calculation method at the B3LYP/6-311+G(d,p) level of theory for the optimized structure of **3** and **10** at the B3LYP/6-31G(d) level of theory. The optimization of **10** with *exo*- or *endo*-oriented substituents was carried out at the B3LYP/6-31G(d) level of theory. The energy difference between the *exo* and the *endo* was calculated from the zero-point corrected energies. The optimization of the bowl and flat structures of **1**, **3**, and **4** was carried out at the B3LYP or M05-2X level of theory with a range of basis sets (6-31G(d), 6-311G(d,p), 6-31++G(d,p), 6-311+G(d), 6-311+G(d,p), and cc-pVDZ), and those of **12**–**18** were calculated at the B3LYP/6-311+G(d,p) level of theory. The flat structure has been characterized as the transition state with one imaginary frequency corresponding to the bowl inversion for these sumanenes. The bowl-inversion energies were calculated from the difference of the zero-point corrected energies of the bowl structure and the flat structure. The interaction energy of benzene-cyclopentadiene complex and natural bond orbital (NBO) analysis of methylsumanene and methylcorannulene were carried out at the MP2/cc-pVDZ level of theory.

Transient Optical Spectroscopy. Compounds were dissolved at 30 mmol dm^{-3} in methyltetrahydrofuran (spectroscopic grade, Dojin Chemical Co., Ltd.). The solutions were placed in quartz cells with a 2-cm optical path, deaerated by

bubbling argon for 15 min, and irradiated by an electron pulse from a linear accelerator (Osaka University). Other details of the transient spectroscopy have been described elsewhere.²² A typical instrument function was ≈ 8 ns.

Support for this work was generously provided by MEXT, JST, the Tokuyama Foundation, the Ishikawa Carbon Foundation, the Asahi Glass Foundation, and the Sumitomo Foundation. We thank Ms. Sachiko Nakano for her technical support.

Supporting Information

Stereodescriptor system for chiral buckybowl, experimental procedures, characterization data for all new compounds, determination of bowl inversion energy of **3** and **4** by CD spectra, chiral HPLC analysis of **10** and **4**, CD spectra of **3** and **10** by TD-DFT calculation, and ¹H and ¹³C NMR spectra. This material is available free of charge on the web at <http://www.csj.jp/journals/bcsj/>.

References

- For recent reviews: a) S. Higashibayashi, H. Sakurai, *Chem. Lett.* **2011**, *40*, 122. b) T. Amaya, T. Hirao, *Chem. Commun.* **2011**, *47*, 10524. c) A. Sygula, *Eur. J. Org. Chem.* **2011**, 1611. d) A. S. Filatov, M. A. Petrukhina, *Coord. Chem. Rev.* **2010**, *254*, 2234. e) Y.-T. Wu, J. S. Siegel, *Chem. Rev.* **2006**, *106*, 4843. f) V. M. Tsefrikas, L. T. Scott, *Chem. Rev.* **2006**, *106*, 4868. g) A. Sygula, P. W. Rabideau, in *Carbon-Rich Compounds: From Molecules to Materials*, ed. by M. M. Haley, R. R. Tykwinski, Wiley-VCH, Weinheim, **2006**, pp. 529–565. doi:10.1002/3527607994.ch12.
- For recent studies: a) A. V. Zabula, S. N. Spisak, A. S. Filatov, A. Yu. Rogachev, M. A. Petrukhina, *Angew. Chem., Int. Ed.* **2011**, *50*, 2971. b) D. Bandera, K. K. Baldrige, A. Linden, R. Dorta, J. S. Siegel, *Angew. Chem., Int. Ed.* **2011**, *50*, 865. c) A. Ueda, K. Ogasawara, S. Nishida, T. Ise, T. Yoshino, S. Nakazawa, K. Sato, T. Takui, K. Nakasuji, Y. Morita, *Angew. Chem., Int. Ed.* **2010**, *49*, 6333. d) D. Eisenberg, E. A. Jackson, J. M. Quimby, L. T. Scott, R. Shenhar, *Angew. Chem., Int. Ed.* **2010**, *49*, 7538. e) B. D. Steinberg, E. A. Jackson, A. S. Filatov, A. Wakamiya, M. A. Petrukhina, L. T. Scott, *J. Am. Chem. Soc.* **2009**, *131*, 10537. f) T. Bauert, L. Merz, D. Bandera, M. Parschau, J. S. Siegel, K.-H. Ernst, *J. Am. Chem. Soc.* **2009**, *131*, 3460. g) D. Miyajima, K. Tashiro, F. Araoka, H. Takezoe, J. Kim, K. Kato, M. Takata, T. Aida, *J. Am. Chem. Soc.* **2009**, *131*, 44. h) L. Merz, M. Parschau, L. Zoppi, K. K. Baldrige, J. S. Siegel, K.-H. Ernst, *Angew. Chem., Int. Ed.* **2009**, *48*, 1966.
- For recent theoretical studies: a) D. Vijay, H. Sakurai, G. N. Sastry, *Int. J. Quantum Chem.* **2011**, *111*, 1893. b) J. R. Green, R. C. Dunbar, *J. Phys. Chem. A* **2011**, *115*, 4968. c) L. Zoppi, A. Garcia, K. K. Baldrige, *J. Phys. Chem. A* **2010**, *114*, 8864. d) G. N. Sastry, *THEOCHEM* **2006**, *771*, 141. e) U. D. Priyakumar, M. Punngai, G. P. K. Mohan, G. N. Sastry, *Tetrahedron* **2004**, *60*, 3037. f) G. N. Sastry, U. D. Priyakumar, *J. Chem. Soc., Perkin Trans. 2* **2001**, *30*. g) U. D. Priyakumar, G. N. Sastry, *J. Phys. Chem. A* **2001**, *105*, 4488. h) G. N. Sastry, H. S. P. Rao, P. Bednarek, U. D. Priyakumar, *Chem. Commun.* **2000**, 843.
- H. Sakurai, T. Daiko, T. Hirao, *Science* **2003**, *301*, 1878.
- a) L. T. Scott, M. M. Hashemi, D. T. Meyer, H. B. Warren, *J. Am. Chem. Soc.* **1991**, *113*, 7082. b) L. T. Scott, M. M. Hashemi, M. S. Bratcher, *J. Am. Chem. Soc.* **1992**, *114*, 1920. c) A. Borchardt, A. Fuchicello, K. V. Kilway, K. K. Baldrige, J. S. Siegel, *J. Am. Chem. Soc.* **1992**, *114*, 1921. d) L. T. Scott, P.-C. Cheng, M. M. Hashemi, M. S. Bratcher, D. T. Meyer, H. B. Warren, *J. Am. Chem. Soc.* **1997**, *119*, 10963. e) A. Sygula, P. W. Rabideau, *J. Am. Chem. Soc.* **1999**, *121*, 7800. f) T. J. Seiders, E. L. Elliott, G. H. Grube, J. S. Siegel, *J. Am. Chem. Soc.* **1999**, *121*, 7804. g) A. Sygula, P. W. Rabideau, *J. Am. Chem. Soc.* **2000**, *122*, 6323.
- a) H. Sakurai, T. Daiko, H. Sakane, T. Amaya, T. Hirao, *J. Am. Chem. Soc.* **2005**, *127*, 11580. b) T. Amaya, H. Sakane, T. Muneishi, T. Hirao, *Chem. Commun.* **2008**, 765. c) T. Amaya, T. Nakata, T. Hirao, *J. Am. Chem. Soc.* **2009**, *131*, 10810. d) T. Amaya, S. Seki, T. Moriuchi, K. Nakamoto, T. Nakata, H. Sakane, A. Saeki, S. Tagawa, T. Hirao, *J. Am. Chem. Soc.* **2009**, *131*, 408. e) T. Amaya, H. Sakane, T. Hirao, *Angew. Chem., Int. Ed.* **2007**, *46*, 8376. f) H. Sakane, T. Amaya, T. Moriuchi, T. Hirao, *Angew. Chem., Int. Ed.* **2009**, *48*, 1640. g) T. Amaya, W.-Z. Wang, H. Sakane, T. Moriuchi, T. Hirao, *Angew. Chem., Int. Ed.* **2010**, *49*, 403. h) P. Zanello, S. Fedi, F. F. de Biani, G. Giorgi, T. Amaya, H. Sakane, T. Hirao, *Dalton Trans.* **2009**, 9192. i) T. Amaya, K. Mori, H.-L. Wu, S. Ishida, J. Nakamura, K. Murata, T. Hirao, *Chem. Commun.* **2007**, 1902.
- a) K. Imamura, K. Takimiya, T. Otsubo, Y. Aso, *Chem. Commun.* **1999**, 1859. b) S. Furukawa, J. Kobayashi, T. Kawashima, *J. Am. Chem. Soc.* **2009**, *131*, 14192. c) S. Furukawa, J. Kobayashi, T. Kawashima, *Dalton Trans.* **2010**, *39*, 9329. d) M. Saito, T. Tanikawa, T. Tajima, J. D. Guo, S. Nagase, *Tetrahedron Lett.* **2010**, *51*, 672. e) T. Tanikawa, M. Saito, J. D. Guo, S. Nagase, *Org. Biomol. Chem.* **2011**, *9*, 1731.
- a) S. Higashibayashi, H. Sakurai, *J. Am. Chem. Soc.* **2008**, *130*, 8592. b) R. Tsuruoka, S. Higashibayashi, T. Ishikawa, S. Toyota, H. Sakurai, *Chem. Lett.* **2010**, *39*, 646.
- For racemic synthesis of C₃ symmetric chiral hemi-fullerene: a) A. H. Abdourazak, Z. Marcinow, A. Sygula, R. Sygula, P. W. Rabideau, *J. Am. Chem. Soc.* **1995**, *117*, 6410. b) S. Hagen, M. S. Bratcher, M. S. Erickson, G. Zimmermann, L. T. Scott, *Angew. Chem., Int. Ed. Engl.* **1997**, *36*, 406. For racemic synthesis of corannulene derivatives, see Ref. 1 and following reference: c) Y.-T. Wu, T. Hayama, K. K. Baldrige, A. Linden, J. S. Siegel, *J. Am. Chem. Soc.* **2006**, *128*, 6870.
- Siegel and co-workers recently reported dynamic enantioselective complexation of racemic pentamethylcorannulene with enantiopure metal complexes under equilibrium through bowl inversion. See Ref. 2b.
- T. J. Seiders, K. K. Baldrige, G. H. Grube, J. S. Siegel, *J. Am. Chem. Soc.* **2001**, *123*, 517.
- The stereodescriptor system, (C) and (A), for the absolute configuration of chiral buckybowl in this article is based on fullerene nomenclature. See Supporting Information and following reference: a) C. Thilgen, F. Diederich, *Chem. Rev.* **2006**, *106*, 5049. Another stereodescriptor system was proposed in the following reference: b) M. A. Petrukhina, K. W. Andreini, L. Peng, L. T. Scott, *Angew. Chem., Int. Ed.* **2004**, *43*, 5477.
- a) S. Higashibayashi, H. Sakurai, *Chem. Lett.* **2007**, *36*, 18. b) A. F. G. M. Reza, S. Higashibayashi, H. Sakurai, *Chem.—Asian J.* **2009**, *4*, 1329. c) S. Higashibayashi, A. F. G. M. Reza, H. Sakurai, *J. Org. Chem.* **2010**, *75*, 4626.
- The relative configuration of a substituent at the benzylic position of sumanenes to the bowl structure is expressed by *exo* or *endo*. The *exo* or *endo* is defined to be a substituent directing to the convex face or the concave face of the bowl structure, respectively.

- 15 a) M. A. Spackman, J. J. McKinnon, D. Jayatilaka, *CrystEngComm* **2008**, *10*, 377. b) S. E. Wheeler, *J. Am. Chem. Soc.* **2011**, *133*, 10262.
- 16 O. Takahashi, Y. Kohno, S. Iwasaki, K. Saito, M. Iwaoka, S. Tomoda, Y. Umezawa, S. Tsuboyama, M. Nishio, *Bull. Chem. Soc. Jpn.* **2001**, *74*, 2421.
- 17 a) A. S. Reddy, G. M. Sastry, G. N. Sastry, *Proteins* **2007**, *67*, 1179. b) A. S. Reddy, H. Zipse, G. N. Sastry, *J. Phys. Chem. B* **2007**, *111*, 11546. c) J. S. Rao, H. Zipse, G. N. Sastry, *J. Phys. Chem. B* **2009**, *113*, 7225.
- 18 R. C. Haddon, *J. Am. Chem. Soc.* **1987**, *109*, 1676.
- 19 A. Bondi, *J. Phys. Chem.* **1964**, *68*, 441.
- 20 a) A. Acharya, S. Seki, A. Saeki, Y. Koizumi, S. Tagawa, *Chem. Phys. Lett.* **2005**, *404*, 356. b) A. Acharya, S. Seki, Y. Koizumi, A. Saeki, S. Tagawa, *J. Phys. Chem. B* **2005**, *109*, 20174.
- 21 a) S. Seki, Y. Kunimi, K. Nishida, Y. Yoshida, S. Tagawa, *J. Phys. Chem. B* **2001**, *105*, 900. b) S. Seki, Y. Koizumi, T. Kawaguchi, H. Habara, S. Tagawa, *J. Am. Chem. Soc.* **2004**, *126*, 3521. c) K. Okamoto, S. Seki, S. Tagawa, *J. Phys. Chem. A* **2006**, *110*, 8073.
- 22 S. Seki, Y. Yoshida, S. Tagawa, K. Asai, *Macromolecules* **1999**, *32*, 1080.
- 23 *CrystalClear: Crystal Structure Analysis Package*, Rigaku and Rigaku/MSC, The Woodlands, TX 77381, USA, **2007**.
- 24 R. Caliendo, B. Carrozzini, G. L. Cascarano, L. De Caro, C. Giacobozzo, A. Mazzone, D. Siliqi, *J. Appl. Crystallogr.* **2008**, *41*, 548.
- 25 *CrystalStructure: Crystal Structure Analysis Package*, Rigaku and Rigaku/MSC, The Woodlands, TX 77381, USA, **2007**.
- 26 a) M. J. Frisch, G. W. Trucks, H. B. Schlegel, G. E. Scuseria, M. A. Robb, J. R. Cheeseman, J. A. Montgomery, Jr., T. Vreven, K. N. Kudin, J. C. Burant, J. M. Millam, S. S. Iyengar, J. Tomasi, V. Barone, B. Mennucci, M. Cossi, G. Scalmani, N. Rega, G. A. Petersson, H. Nakatsuji, M. Hada, M. Ehara, K. Toyota, R. Fukuda, J. Hasegawa, M. Ishida, T. Nakajima, Y. Honda, O. Kitao, H. Nakai, M. Klene, X. Li, J. E. Knox, H. P. Hratchian, J. B. Cross, V. Bakken, C. Adamo, J. Jaramillo, R. Gomperts, R. E. Stratmann, O. Yazyev, A. J. Austin, R. Cammi, C. Pomelli, J. W. Ochterski, R. L. Martin, K. Morokuma, V. G. Zakrzewski, G. A. Voth, P. Salvador, J. J. Dannenberg, S. Dapprich, A. D. Daniels, Ö. Farkas, J. B. Foresman, J. V. Ortiz, J. Cioslowski, D. J. Fox, *Gaussian 09, Revision A.1*, Gaussian, Inc., Wallingford CT, **2009**.